

Trace and rare earth elements constraints on the sources of the Yunfeng paleo-karstic bauxite deposit in the Xiuwen-Qingzhen area, Guizhou, China

Yongzhen Long^{a,b,*}, Guoxiang Chi^c, Jianping Liu^{a,b}, Zhongguo Jin^d, Tangen Dai^{a,b}

^a Key Laboratory of Metallogenic Prediction of Nonferrous Metals and Geological Environment Monitoring, Ministry of Education, Central South University, Changsha 410083, China

^b School of Geosciences and Info-Physics, Central South University, Changsha 410083, China

^c Department of Geology, University of Regina, Saskatchewan S4S 0A2, Canada

^d Non-Ferrous Metals and Nuclear Industry Geological Exploration Bureau of Guizhou, Guiyang 550005, China

ARTICLE INFO

Keywords:

Paleo-karstic
Bauxite deposit
Provenance
Uranium
Yunfeng
Guizhou

ABSTRACT

A number of Carboniferous paleo-karstic bauxite deposits occur in the Xiuwen-Qingzhen area, central Guizhou Province, which constitute an important part of the central Guizhou-Southern Chongqing bauxite belt in southwestern China. These deposits consist of lenticular and stratiform orebodies hosted in the Lower Carboniferous Jiujialu Formation, which lies unconformably above carbonate rocks (mainly dolomite) of the Middle and Upper Cambrian Loushanguan Group, Shilengshui Formation and Lower Cambrian Qingxudong Formation. Although it is generally agreed that the bauxite resulted from weathering of Cambrian rocks below the unconformity, it remains unclear whether the carbonates alone can provide sufficient material for the formation of the deposits. In this study, we examined the mineralogy and major, trace and rare earth elements geochemistry of bauxite and bauxitic clays from the Yunfeng deposit in the Xiuwen-Qingzhen area and compared them to previously published data of a paleo-weathering profile consisting of Loushanguan dolomite underlying the sub-Carboniferous unconformity and the “Black Rock Sequence” of the Lower Cambrian Niutitang Formation, in order to evaluate the sources of the bauxite. The bauxite ores are composed of diaspore as the main ore mineral, along with small amounts of pyrite, arsenopyrite, galena, stibnite, xenotime and uranium-bearing minerals, and are characterized by high contents of uranium and phosphorus. Chondrite-normalized REE patterns and various bivariate diagrams commonly used to study the provenance of bauxite including Eu/Eu* vs TiO₂/Al₂O₃, Eu/Eu* vs Sm/Nd, TiO₂ vs Al₂O₃, TiO₂/Th, Th vs Ta, Th vs Nb and Nb vs Ta suggest that the Loushanguan dolomite and the Niutitang “Black Rock Sequence” are both potential source rocks. However, a comparison in U and Th contents between the paleo-weathering profile of the Loushanguan dolomite and the bauxite samples suggests that the dolomite alone cannot provide the materials for the bauxite ores. Instead, the “Black Rock Sequence” may have contributed most of the ore-forming materials, which are mainly transported from source regions where the Niutitang Formation was exposed, weathered and eroded. Therefore, the Yunfeng bauxite deposit is of mixed autochthonous and allochthonous origin.

1. Introduction

Karstic bauxite deposits form as a result of accumulation of weathering products in depressions on more or less karstified carbonates surface (Bárdossy and Aleva, 1990; Bogatyrav et al., 2009). They are divided into autochthonous, para-autochthonous, allochthonous and para-allochthonous subtypes (Bárdossy, 1982; Combes et al., 1993; Hanlıç, 2013; Ahmadnejad et al., 2017). Most of the karstic bauxite deposits in China (about 73%) were formed in the Paleozoic (paleo-karstic) and are widely spread within the southwestern South China

Block (SCB) and the North China Craton (Wu et al., 2006; USGS, 2009; Gu et al., 2013; Zhang et al., 2013; Ling et al., 2015, 2017; Liu et al., 2017). According to the data by the end of 2008, more than 155 Mt of bauxite resources are present in Guizhou province, which is located in southwestern SCB (USGS, 2009; Gu et al., 2013; Ling et al., 2013, 2015, 2017). These bauxite resources are mainly of karstic type, and are distributed in several mineralization districts in Guizhou Province including Xiuwen-Qingzhen, Zunyi-Wengan, Zhengan-Daozhen, and Kaili-Huangping (Fig. 1a).

For lateritic-type bauxites overlying aluminosilicate rocks, the ore is

* Corresponding author at: Key Laboratory of Metallogenic Prediction of Nonferrous Metals and Geological Environment Monitoring, Ministry of Education, Central South University, Changsha 410083, China.

E-mail address: jilllongyz@qq.com (Y. Long).

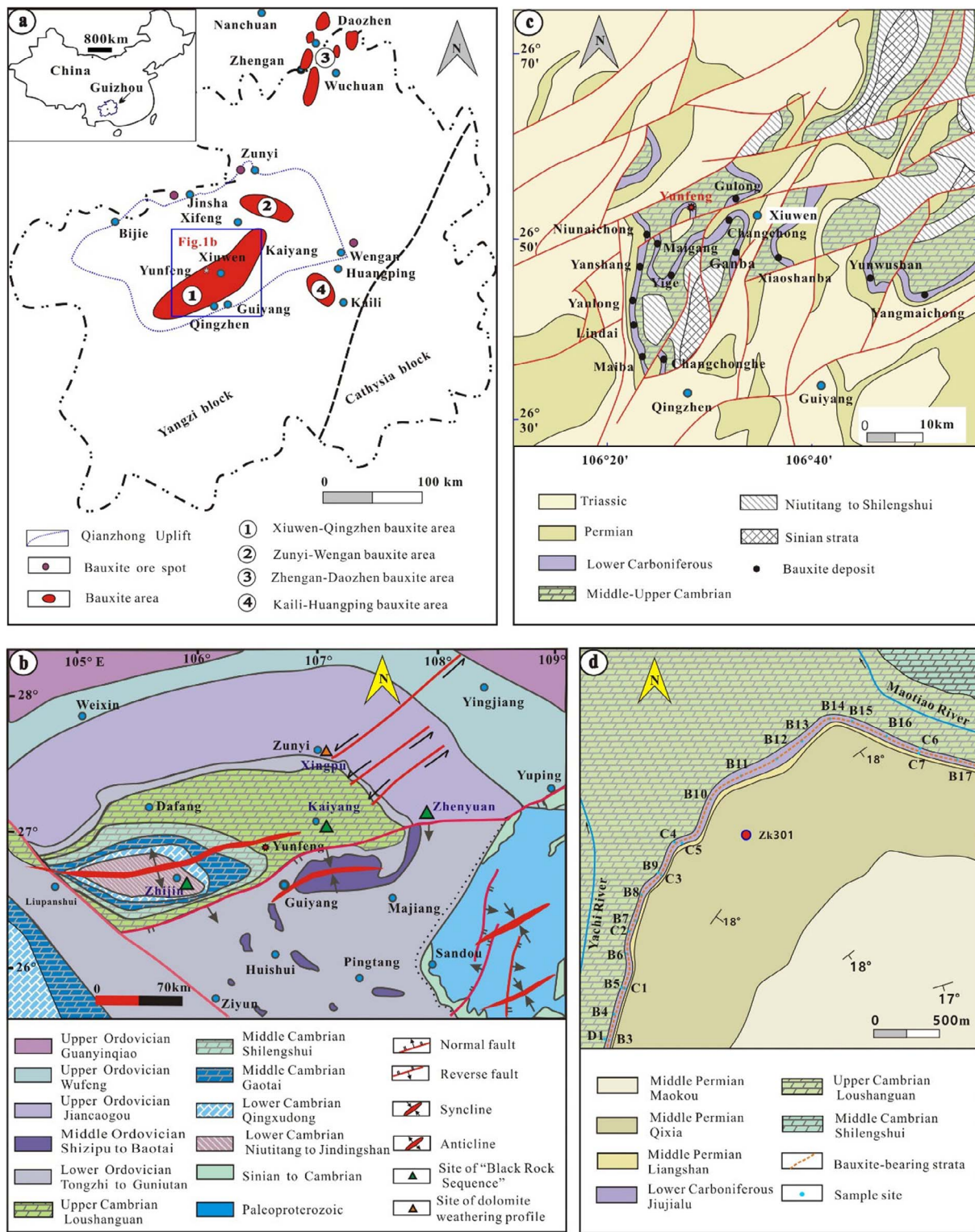


Fig. 1. (a) Sketch map showing the distribution of bauxite deposits in Guizhou province (After Li et al., 2014); (b) Paleostructure map of Duyun movement in central Guizhou (from Deng et al., 2010a,b); (c) Sketch geological map of the Xiuwen-Qingzhen bauxite area (After Guizhou Bureau of Geology and Minerals, 1987) and (d) Geological map of the Yunfeng bauxite deposit (after Yunfeng Mining Company, unpublished data, 2013).

generally inferred to be derived from weathering of the bedrocks (Mutakyahwa et al., 2003; Hou et al., 2017) i.e. of autochthonous origin. However, for karstic (especially paleo-karstic) bauxite deposits, which are underlain by carbonate rocks, controversies generally exist between autochthonous and allochthonous origins. The formation of the allochthonous bauxite deposits involves multiple processes

including weathering, transportation, deposition, diagenesis, and supergene leaching stages. The exact precursor rocks from which the bauxites were derived are difficult to determine (Deng et al., 2010a,b; Wei et al., 2013; Liu et al., 2017; Ahmadnejad et al., 2017; Hou et al., 2017; Ling et al., 2017). Various methods have been used to address this problem, including immobile elements ratios (MacLean et al., 1997;

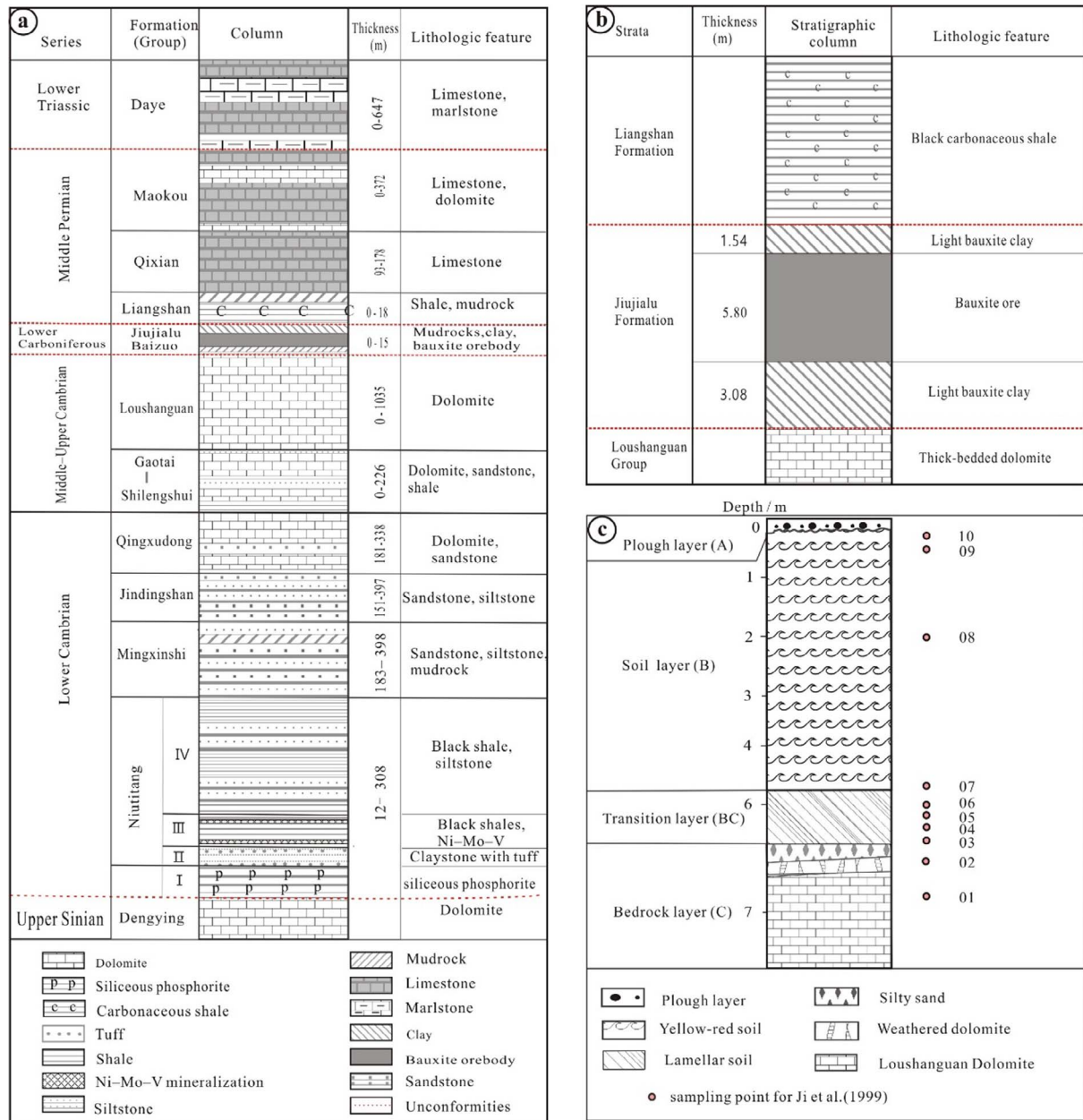


Fig. 2. (a) Lithostratigraphic column of Yunfeng bauxite, central Guizhou Province (modified from Guizhou Bureau of Geology and Minerals, 1987; Pi et al., 2013; Yang et al., 2013; Wang and Zhang, 2016); (b) Lithostratigraphic column for ore-bearing strata of a typical drilling hole (ZK301 in Fig. 1d, after Yunfeng Mining Company, unpublished data, 2013); (c) Geological section of the Upper Cambrian Loushanguan Group dolomite weathering profile, Xinpu, Zunyi, Guizhou Province (From Ji et al., 1999).

Mameli et al., 2007; Wang et al., 2013; Zamanian et al., 2016; Ahmadnejad et al., 2017; Liu et al., 2017), REE patterns (Mongelli, 1997; Wang et al., 2012; Li et al., 2013; Zamanian et al., 2016), Eu-anomaly vs $\text{TiO}_2/\text{Al}_2\text{O}_3$ (Mameli et al., 2007; Ahmadnejad et al., 2017), Eu-anomaly vs Sm/Nd diagrams (Mongelli et al., 2014; Ahmadnejad et al., 2017), the so-called accumulation coefficient of trace elements (Özlu, 1983), and vertical variations in mineral and chemical composition as well as Th/U ratios across bauxite bodies (Lukas et al., 1983). Nevertheless, many of the provenance studies of paleo-karstic bauxite deposits remain nonconclusive due to complexities related to prolonged weathering and diagenesis.

In the case of the bauxite deposits in central Guizhou Province, dolomite of the Middle to Upper Cambrian Loushanguan Group that underlies most bauxite deposits has been suggested as the major source rock (e.g., Li et al., 2014 and Liu and Liao, 2014). However, various other source rocks have also been proposed for different deposits, for

example, dolomite of the Middle Cambrian Shilengshui Formation for the overlying Lindai deposit (Ling et al., 2013, 2017), and dolomite of the Lower Cambrian Qingxudong Formation for the overlying Heitutian deposit (Yang et al., 2014). All these studies imply that the bauxite deposits in central Guizhou Province are of autochthonous nature. In contrast, Yang et al. (2014) speculated that the bauxite in central Guizhou Province may have been derived from weathering of multiple source rocks present below the sub-Carboniferous unconformity, in addition to those immediately underlying the bauxite deposits, and Gu et al. (2013) and Huang et al. (2014) suggest that the bauxite deposits in the Wuchuan–Zheng'an–Daozhen district in northern Guizhou Province were sourced from Neoproterozoic mafic igneous rocks and Mesoproterozoic mafic-ultramafic intrusions in the basement, both implying that the bauxite deposits are of allochthonous origin. Thus, there are two contrasting opinions about the origins of the paleo-karstic bauxite deposits in Guizhou Province: autochthonous versus

allochthonous.

This paper tackles the provenance problem of the paleo-karstic bauxite deposits in central Guizhou Province through examination of the Yunfeng bauxite deposit. This deposit, hosted by the Lower Carboniferous Jiujialu Formation and unconformably underlain by dolomite of the Middle to Upper Cambrian Loushanguan Group, is one of the most representative paleo-karstic bauxite deposits in the Xiuwen-Qingzhen district in central Guizhou Province (Fig. 1a).

We examined the petrography and major, trace and rare earth element geochemistry, and use them to investigate the possible source rocks of the bauxite. Particular attention was paid to determining whether the bauxite was derived from the dolomite below the orebodies (autochthonous origin) or was transported from distal sources (allochthonous origin). The methods used and the conclusions reached may be extended to other similar bauxite deposits in the same region and elsewhere.

2. Regional and local geology

2.1. Geological background

The Xiuwen-Qingzhen bauxite area in central Guizhou Province (Qianzhong), southwestern China (Fig. 1a) represents the largest bauxite district in the Qianzhong-Southern Chongqing bauxite belt, which is one of the most important bauxite belts in China (Guizhou Bureau of Geology and Minerals, 1987; Liu, 2001; Deng et al., 2010a,b; Li et al., 2014). The area is situated in the Guiyang Complex Tectonic Deformation Zone in the Qianzhong Uplift (Fig. 1b), which is located within the Yangtze Block in South China (Fig. 1a) (Guizhou Bureau of Geology and Minerals, 1987; Li et al., 2014).

The stratigraphic succession of the Xiuwen-Qingzhen area consists of, from the oldest to the youngest, the Sinian (Neoproterozoic) Dengying Formation, Lower Cambrian Niutitang “Black Rock Sequence”, Mingxinsi, Jindingshan, and Qingxudong formations, Middle-Upper Cambrian Gaotai, Shilengshui formations and Loushanguan Group, Lower Carboniferous Jiujialu and Baizuo formations, Permian Liangshan, Qixia and Maokou formations, and Lower-Triassic Daye Formation (Tian et al., 2006; Yang et al., 2012; Pi et al., 2013; Yang et al., 2013; Huang et al., 2014; Liu et al., 2015; Zhang et al., 2016) (Fig. 1b, c and d; Fig. 2a). The Dengying, Qingxudong, Gaotai and Shilengshui formations and the Loushanguan Group are made of carbonates, mainly dolomite. The Mingxinsi and Jindingshan formations comprise sandstone and siltstone intercalated with shale, mudrock and limestone. The Niutitang “Black Rock Sequence” is divided into four units, which are, from the bottom to the top: (I) brownish to black siliceous phosphorite unconformably overlying the dolomite of the Dengying Formation, (II) grey to black pyrite-rich claystone intercalated with grey to black tuff, (III) black shales containing pyrite, organic debris, phosphatic nodules, and Ni-Mo-V mineralization, and (IV) black shale and silty shale (Pi et al., 2013; Yang et al., 2013; Yi and Zhao, 2014) (Fig. 2a). The Jiujialu Formation consists of mudrocks transitional to bauxite-rich clay units and bauxite orebodies, and the Baizuo Formation is comprised of argillaceous dolomite. They are unconformably overlying the dolomite of the Loushanguan Group, Shilengshui Formation (Ling et al., 2015, 2017), or Qingxudong Formation (Yang et al., 2014). The Permian rocks consist of black carbonaceous shale, mudrock and sandstone (Liangshan Formation), limestone (Qixia Formation), and limestone and thin layers of dolomitic limestone (Maokou Formation), and the Triassic rocks are made of sandy, silty, and dolomitic limestones (Daye Formation) (Guizhou Bureau of Geology and Minerals, 1987; Huang et al., 2014; Liu et al., 2015) (Fig. 2a).

The Xiuwen-Qingzhen area experienced multiple orogenies following the formation of the Sinian to early Cambrian sedimentation. During the late Cambrian period, this region experienced a major transgression-regression cycle in relation to the Yunan orogeny that

resulted in the Qianzhong uplift, and some areas such as Xuanwei, Northeast Yunnan Province, were uplifted to become paleo-lands (Guizhou Bureau of Geology and Minerals, 1987; Mei et al., 2006). The subsequent Duyun orogeny in the Ordovician further uplifted the central Guizhou region (Fig. 1b). By the time of Devonian, the region became a peneplain, after more than 100 million years of weathering and erosion (Deng et al., 2010a,b; Ling et al., 2015). The transgression of the paleo-South China Sea from south to north resulted in the deposition of early Carboniferous sedimentary rocks (Guizhou Bureau of Geology and Minerals, 1987; Liu, 2001; Ling et al., 2015). The region was subsequently uplifted again during the Ziyun Movement in Late Carboniferous, followed by a transgression in Middle Permian forming marine carbonate sedimentation. During the late Permian to early Triassic stage, this region experienced another regression-transgression cycle in relation with the Dongwu orogeny, resulting in the deposition of the Lower Triassic Daye Formation that unconformably overlie the Permian rocks (Fig. 2a) (Guizhou Bureau of Geology and Minerals, 1987).

2.2. Geological characteristics of the Yunfeng bauxite deposit

The Yunfeng bauxite deposit is located in the northwest of the Xiuwen-Qingzhen bauxite district (Fig. 1c). It consists of lenticular and stratiform orebodies hosted in the Lower Carboniferous Jiujialu Formation, which extends over several kilometers (Fig. 1d). The ore-bearing strata overlie unconformably carbonate rocks (mainly dolomite) of the Upper Cambrian Loushanguan Group and underlie the Middle Permian Liangshan Formation (Fig. 2a and b). The unconformity surface is undulatory, and the bauxite ores fill the depressions and sinkholes in the footwall dolomite (Fig. 3a).

The ore-bearing interval is generally divided into three layers as shown in Fig. 2b: an upper layer of light bauxitic clay, a middle layer of bauxite orebodies, and a lower layer of light bauxitic clay. The thickness ranges from 1.5 to 6 m, 3 to 6 m, and 0 to 3.1 m, for the upper, middle, and lower layer, respectively. The bauxitic clays are composed of illite, boehmite, kaolinite and iron minerals. The bauxite ores show various colors from light grey to dark grey (Fig. 3a-e show), and are composed mainly of diaspore, illite, kaolinite, goethite/limonite and pyrite (Table 2). The ores have earthy (Fig. 3h), compact (Fig. 3b), pisolithic and oolitic (Fig. 3d and e, Fig. 4a) as well as clastic (Fig. 3c, f and g) structures. The clasts of the bauxite ores generally exhibit median to well-rounded shapes, indicating that they were transported over significant distances (Gao et al., 1992; Ling et al., 2015).

3. Sampling and analytical methods

Seventeen representative bauxite ore samples (B1 to B17), seven bauxitic clay ($\text{Al}_2\text{O}_3/\text{SiO}_2 < 1.8$ or $\text{Al}_2\text{O}_3 < 40 \text{ wt\%}$) samples (C1 to C7), and one semi-weathered dolomite sample from the Upper Cambrian Loushanguan Group (D1), were collected from both outcrops and underground tunnel of the Yunfeng deposit (Fig. 1d; Table 1). Geochemical data of a weathering profile of the Loushanguan dolomite were obtained from Xinpu, Zunyi (see Fig. 1b and Fig. 2c for location) by Ji et al. (1999), and the data for the “Black Rock Sequence” were obtained from Kaiyang by Zhang et al. (2016), from Zhijin by Wang and Zhang (2016) and from Zhenyuan by Yang et al. (2013) (see Fig. 1b for locations).

The mineralogical compositions of the bauxite ores and bauxitic clays from the Yunfeng deposit were investigated by petrographic examination of thin (30 μm) and thick (120–150 μm) polished sections, X-ray diffraction (XRD) analysis of 200 mesh rock powders, and electron probe microanalysis (EPMA) of polished sections. The XRD studies were performed with a Rigaku D/Max-2200 model instrument using a Cu K α tube with settings of 40 kV and 20 mA; the scanning scope, step length and speed were set to 2°–60°, 0.04° and 10°/min, respectively. Semi-quantitative estimation of mineral components was conducted

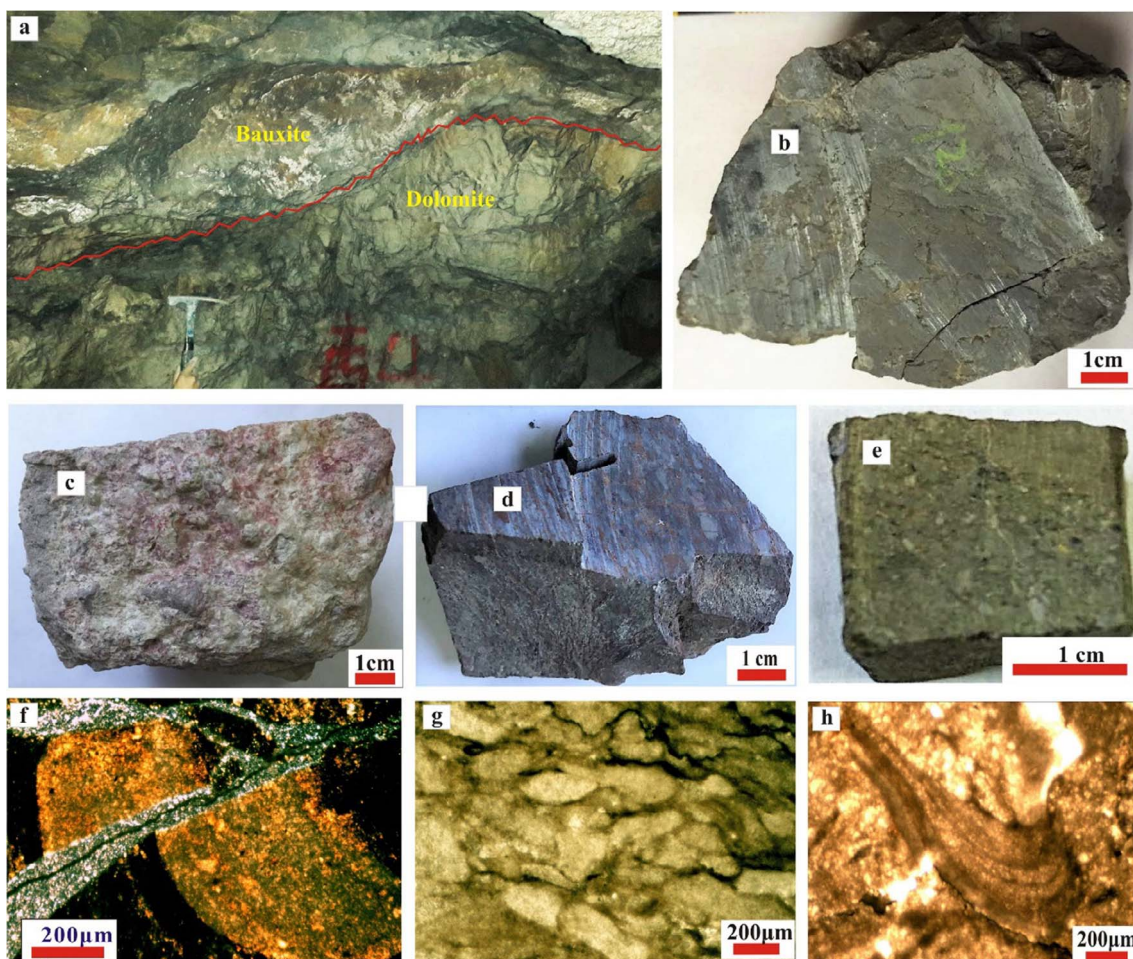


Fig. 3. Photos and photomicrographs showing the features of the Yunfeng bauxite, Qingzhen, Guizhou, China. (a) A lenticular orebody occurring in a karstic depression of dolomite of the Loushanguan Group; (b) Gray compact bauxite; (c) Light grey to reddish clastic bauxite; (d) Steel gray to dark rusty red ferruginous bauxite with pisolithic and oolitic textures; (e) Gray pisolitic and oolitic bauxite; (f) An elliptical rock debris cut by a micro fault (thin sections in polarized light); (g) Photomicrograph of bauxite grains with sub-rounded shapes (thin section in polarized light); (h) Argillaceous bauxite with plastic debris (thin section in polarized light).

using the K value method. The EPMA analysis was performed using a Shimadzu EPMA-1600 Scanning Electron Microscope (SEM) equipped with a wavelength dispersive spectrometer (WDS) and EDAX Genesis energy dispersive spectrometer (EDS). Silicates, oxides, and pure elements were used as standards (analytical errors are 1% for major elements and 3% for minor elements). Back scattered electron images were obtained at an accelerating voltage of 12 kV and a beam current of $\sim 10 \mu\text{A}$. The XRD and EPMA analyses were conducted at the Key Laboratory of Metallogenetic Prediction of Nonferrous Metals and Geological Environment Monitoring, Ministry of Education of China.

The bauxite, bauxitic clay and dolomite samples were ground to finer than 200 meshes for whole-rock geochemical analysis. Major elements (Al_2O_3 , Fe_2O_3 , SiO_2 , TiO_2 , P_2O_5) were analyzed with a wet chemistry method, with data quality controlled by duplicated samples and international standard samples (GBW07179, GBW07405) yielding precision better than 5%. The analysis was performed at the Analytical Detection Central of Changsha Research Institute of Mining and Metallurgy, Hunan, China. Trace elements and rare earth elements were analyzed by an inductively coupled plasma mass spectrometer (VG PQ Excell ICP-MS, Thermo Electron Corporation) at the Key Laboratory of Metallogenetic Prediction of Nonferrous Metals, Hunan, China, following the procedure described in Qi et al. (2000). Forty (40) mg of each sample was dissolved in a high-pressure Teflon beaker for 24 h at 190°C using $\text{HF} + \text{HNO}_3$ mixture. Rh was used as an internal standard to monitor signal drift during ICP-MS analysis (Qi et al., 2000; Ling et al., 2015), and international standards (AMH-1, OU-6, and GBPG-1)

were used to control the analytical quality. The relative standard deviation (RSD) of the REE and trace elements analysis was below 4%. Statistical treatments were conducted for the geochemical results using SPSS 19.0 software.

4. Results

4.1. Mineral components

The results of optical microscopy, XRD and EPMA studies indicate that the bauxitic clays are composed mainly of illite, boehmite and kaolinite, along with small amounts of diaspore, hematite, quartz, rutile, gypsum and siderite (Table 2). The bauxite ores are composed mainly of diaspore and illite, plus minor and variable amounts of kaolinite, goethite, quartz, rutile, chlorite, gypsum and anatase (Table 2; Figs. 3–6).

The bauxite ores also contain trace amounts of pyrite, zircon, stibnite, chalcopyrite, galena, xenotime, uranium-bearing mineral, cobalt-nickel-bearing arsenopyrite and cobalt-bearing pentlandite (Figs. 4–6). The arsenopyrite contains 11.08 wt% Ni and 15.34 wt% Co (Fig. 5a), and the cobalt-bearing pentlandite contains 16.52 wt% Ni and 2.02 wt % Co (Fig. 5b). The undetermined uranium mineral contains 26.67 wt% O, 4.05 wt% As, 4.13 wt% Al, 4.09 wt% Si, 1.05 wt% P, 34.34 wt% U, 21.73 wt% Ti, 2.59 wt% Fe and 1.35 wt% Co (Fig. 6d).

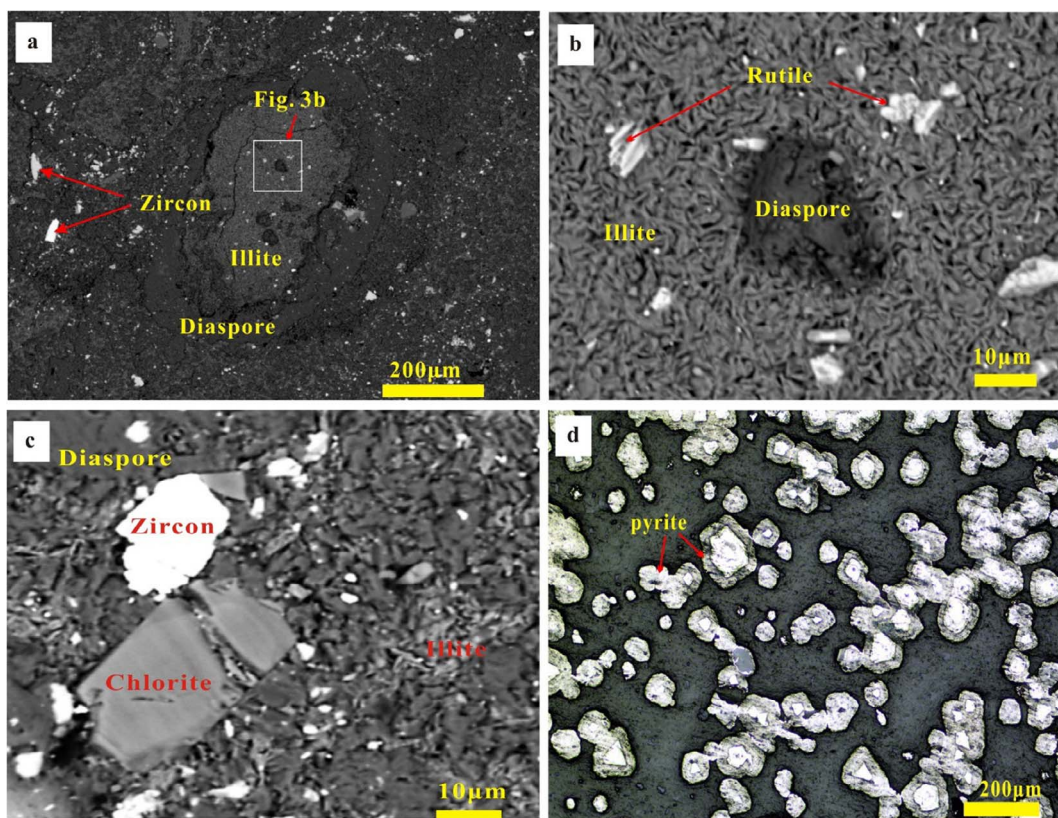


Fig. 4. Backscattered electron (BSE) images and photomicrographs of bauxite ores from the Yunfeng bauxite, Guizhou, China, (a) and (b) Backscattered electron (BSE) images of oolitic bauxite with clastic zircon and rutile; (c) Backscattered electron (BSE) images showing the debris of zircon and chlorite distributed in the matrix of diaspore and illite; (d) Photomicrographs of euhedral pyrite with reaction rim (thick section view under reflected light).

Table 1

List of samples from the Yunfeng bauxite deposit.

Sample No.	Location	Sample characteristics
D1	Lower adit	Semi-weathered dolomite of Loushanguan Group
C1	Main adit	Bauxitic clay
C2	Main adit	Bauxitic clay
C3	Main adit	Gray bauxitic clay
C4	Main adit	Bauxitic clay
C5	Main adit	Bauxitic clay
C6	Main adit	Bauxitic shale
C7	Main adit	Ferruginous bauxitic clay
B1	Outcrop	Earthy bauxite
B2	Outcrop	Compact bauxite
B3	Lower adit	Dark-gray bauxite
B4	Lower adit	Green-gray bauxite
B5	Main adit	White-gray bauxite
B6	Main adit	Clastic and oolitic bauxite
B7	Main adit	Dark-gray bauxite
B8	Main adit	Dark-gray bauxite
B9	Main adit	Dark-gray oolitic bauxite
B10	Main adit	Ferruginous bauxite
B11	Main adit	Gray bauxite
B12	Main adit	Clastic bauxite
B13	Main adit	Earthy bauxite
B14	Main adit	Oolitic bauxite
B15	Main adit	Light green bauxite
B16	Main adit	Lumpy bauxite
B17	Main adit	Compact ferruginous bauxite

4.2. Geochemistry

The analytical values of major, trace, and rare earth elements in 25 representative samples (bauxite ores, bauxitic clays, and semi-weathered carbonate) collected from the Yunfeng bauxite deposit are listed in

Table 3.

4.2.1. Major and trace elements

The geochemical data show that the bauxite ores are mainly composed of Al_2O_3 (51.10–73.6 wt%), SiO_2 (1.56–24.4 wt%), with erratic amounts of Fe_2O_3 (1.11–23.49 wt%), and small amounts of TiO_2 (1.92–5.30 wt%) and P_2O_5 (0.10–1.15 wt%). The content of P_2O_5 (average 0.53) is relatively higher compared to other bauxite deposits in the world (average value ranging from < 0.1 to 0.12 wt%, see Zaravandi et al., 2008; Wang et al., 2010; Wang et al., 2012; Hanilçi, 2013; Liu et al., 2013, 2017; Ahmadnejad et al., 2017). The bauxitic clays contain Al_2O_3 (12.96–50.19 wt%), Fe_2O_3 (1.31–36.91 wt%), SiO_2 (4.38–41.20 wt%) and small amount of TiO_2 (0.94–3.04 wt%) (Table 3).

The bauxite ores and bauxitic clays contain more than 100 ppm of Zr, Cr, Ni, and Sr as well as relatively high concentration of U. The U contents are 18.0–62.4 (average 35.1) ppm for bauxite ores and 9.6–25.3 (average 18.3) ppm for bauxitic clays (Table 3), which is significantly higher than the crustal values (approximately 1–3 ppm, see Cumberland et al., 2016; Taylor and McLennan, 1985).

Correlation analyses (Table 4, Figs. 7 and 8) revealed that Al_2O_3 has moderately positive correlation with U ($R = 0.66$). Both Al_2O_3 and U have medium to high positive correlations with TiO_2 , Nb, Th, Ta and LREE and significant negative correlations with SiO_2 . Bivariant diagrams of Nb vs Ta, TiO_2 vs Nb and TiO_2 vs Ta exhibit high positive correlations. Diagrams of TiO_2 vs Th, TiO_2 vs U and Th vs Nb have medium positive correlations. However, both Al_2O_3 and U have no correlation or weak negative correlation with Zr, Hf and Fe_2O_3 (Table 4, Fig. 7g and Fig. 8b).

4.2.2. Rare earth elements

The bauxite ores are characterized by high ΣREE contents

Table 2

Mineralogy of typical bauxite ores and bauxitic clays (wt.%) as determined by X-ray Diffraction.

Sample	Diasporite	Boehmite	Kaolinite	Illite	Hematite	Quartz	Rutile	Chamosite	Gypsum	Anatase	Siderite
B1	82.85	–	2.40	7.85	0.97	–	3.50	1.46	0.24	0.73	–
B3	78.51	–	3.16	5.44	2.37	4.88	3.76	1.43	0.25	0.20	–
B4	47.04	–	0.34	42.49	0.09	–	3.66	5.39	0.67	0.32	–
B5	84.81	–	1.58	6.55	1.65	0.20	3.06	1.53	0.18	0.44	–
B9	78.21	–	1.14	4.26	6.57	0.24	5.06	3.66	0.62	0.24	–
B11	82.75	–	4.89	4.13	3.91	–	3.56	–	0.34	0.42	–
B12	63.91	–	1.02	26.87	1.79	–	2.55	3.07	0.28	0.51	–
B13	80.56	–	4.96	5.98	2.6	0.58	4.78	–	0.17	0.37	–
B14	63.33	–	0.08	24.77	2.47	2.73	2.96	3.13	0.46	0.07	–
B16	60.61	–	1.75	27.51	1.37	3.15	2.16	3.01	0.28	0.16	–
B17	67.05	–	2.69	19.37	1.75	2.19	4.16	2.15	0.46	0.18	–
C1	3.25	24.56	2.50	58.27	3.30	2.26	2.20	–	3.66	–	–
C4	2.04	7.19	7.25	39.24	–	17.85	1.66	–	3.74	–	15.58
C6	2.40	2.70	68.31	12.00	2.70	8.50	2.54	–	–	0.50	–

(266–2188 ppm), right-inclined REE patterns with erratic LERR/HREE ratios (1.95–21.38 ppm), stable negative Eu anomalies with Eu/Eu^* values of 0.56–0.80, and weak Ce anomalies with variable Ce/Ce^* values of 0.69–1.41, slightly fractionated LREE with $(\text{La}/\text{Sm})_N$ ratios of 2.14–6.25, and flat HREE pattern with $(\text{Gd}/\text{Yb})_N$ ratios of 0.61–1.49 (Fig. 9a). The bauxitic clays have high ΣREE contents (348–994 ppm) and high LREE/HREE ratios (3.00–16.05), negative Eu ($\text{Eu}/\text{Eu}^* = 0.69$ –0.83) and Ce ($\text{Ce}/\text{Ce}^* = 0.65$ –0.98) anomalies, moderately fractionated LREE with $(\text{La}/\text{Sm})_N$ ratios ranging from 1.53 to 10.30 and nearly flat HREE pattern with $(\text{Gd}/\text{Yb})_N$ ratios ranging from 0.78 to

1.76 (Fig. 9b). The weathered dolomite sample (D1) is characterized by low ΣREE content (67 ppm), right-inclined REE pattern with LERR/HREE ratio 5.02, negative Eu anomaly with Eu/Eu^* value of 0.65, and weak Ce anomaly with Ce/Ce^* value of 0.79, slightly fractionated LREE with $(\text{La}/\text{Sm})_N$ ratio of 3.27, and flat HREE pattern with $(\text{Gd}/\text{Yb})_N$ ratio of 1.26 (Fig. 9c). These results are comparable with those from the weathering profile of dolomite of the Loushanguan Group reported by Ji et al. (1999) (Fig. 9c). The significant negative Ce anomalies and low ΣREE contents of the weathered dolomite distinguish them from the bauxite ores and bauxitic clays (Fig. 9a–c). The “Black Rock Sequence”,

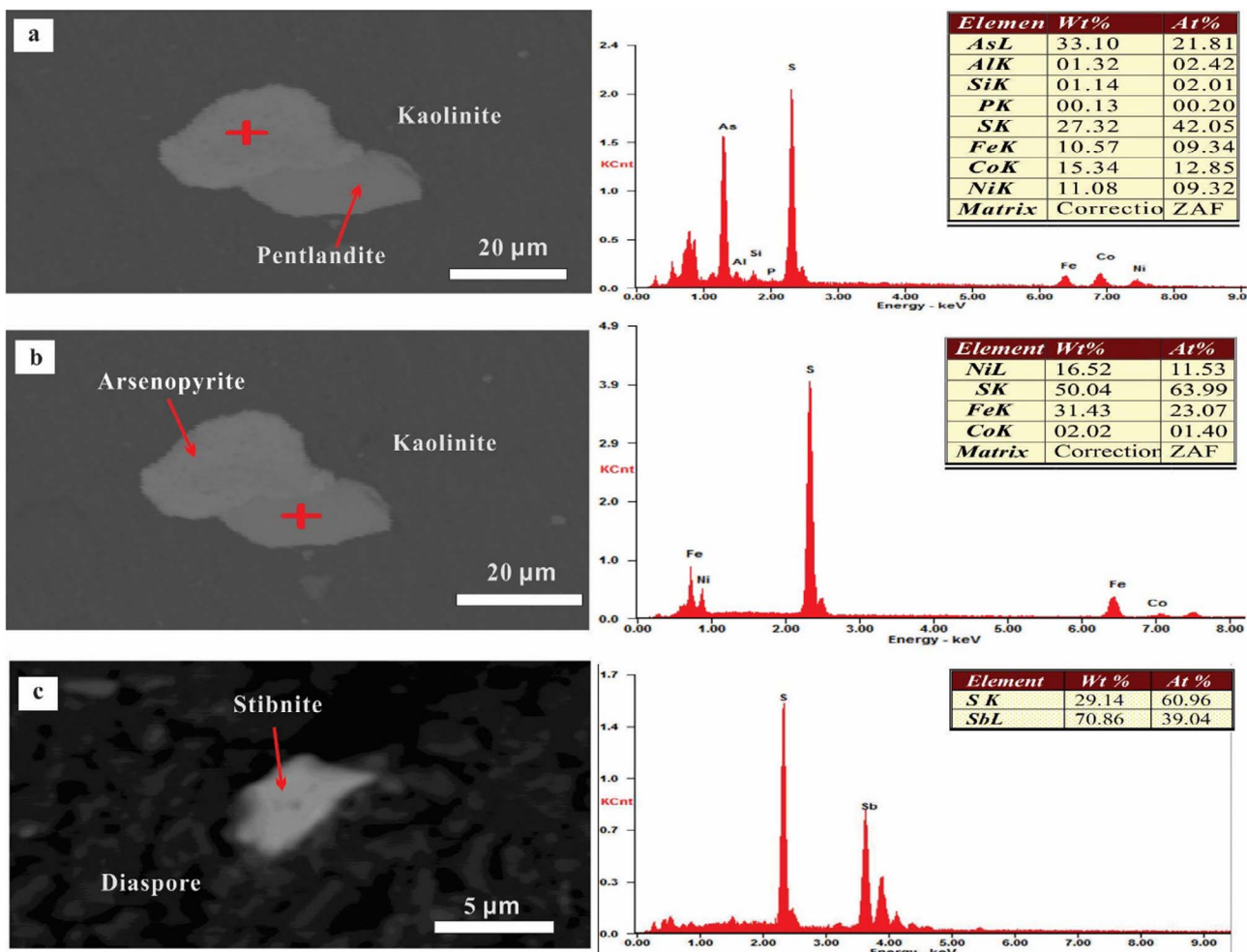


Fig. 5. Backscattered electron (BSE) images and EDS spectrum showing: (a) Cobalt nickel arsenopyrite (red cross); (b) Cobalt-bearing pentlandite (red cross); (c) Stibnite.

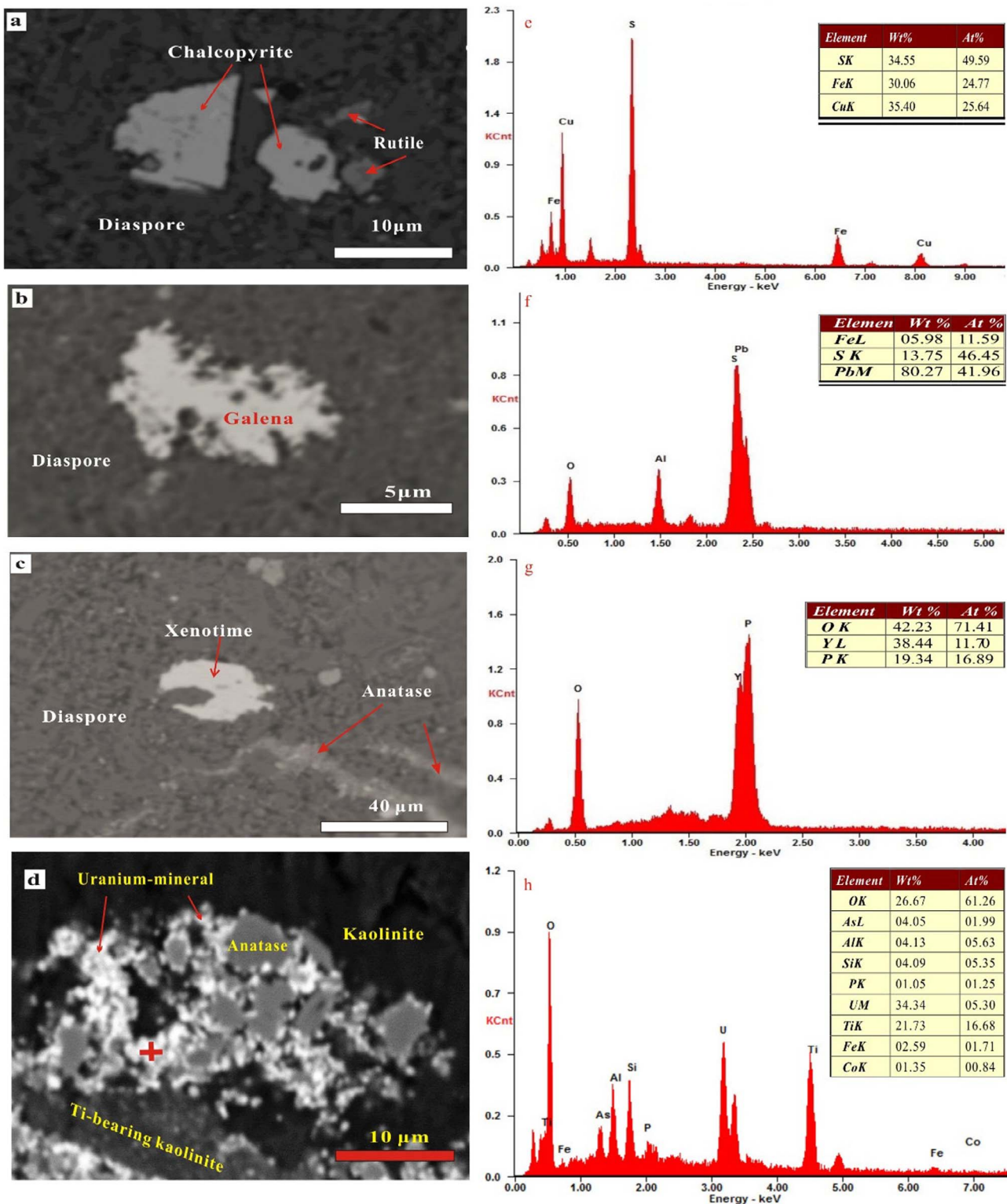


Fig. 6. Backscattered electron (BSE) images and EDS spectrum showing: (a) Chalcopyrite; (b) Galena; (c) Xenotime; (d) Uranium-bearing mineral (red cross).

on the other hand, show overall similar REE patterns as the bauxite ores and bauxitic clays, except for the more prominent negative Ce anomalies and lower LREE fractionation (Fig. 9d).

5. Discussion

Although it is generally agreed that paleo-karstic bauxite deposits resulted from weathering of Al-bearing minerals in ancient geological

times, there are significant uncertainties regarding the source rocks. Various protoliths have been suggested in different deposits, including alluvial mud (Hanilçi, 2013; Dill, 2017), flood basalts and associated felsic magmatic rocks (Deng et al., 2010a,b), volcanic ash or eolian dust intercalated in limestones (Bárdossy and Aleva, 1990; Merino and Banerjee, 2008; Esmaeily et al., 2010; Dill, 2017; Hou et al., 2017), carbonate sequences underlying the bauxite deposits (Ling et al., 2015, 2017; Zamanian et al., 2016; Ahmadnejad et al., 2017), and a mixed

Table 3
Concentrations of major elements (%), trace elements and rare earth elements (ppm) of bauxite ores, bauxitic clays and dolomites from the Yunfeng bauxite deposit

Sample	B1	B2	B3	B4	B5	B6	B7	B8	B9	B11	B12	B13	B14	B15	B16	B17	B18	B19	B20	Average	C1	C2	C3	C4	C5	C6	C7	Average	D1
Al ₂ O ₃	73.03	55.22	68.88	56.75	73.66	52.75	67.49	70.39	64.95	72.9	64.72	55.02	63.12	66.21	51.49	51.1	58.65	62.73	45.1	50.19	12.96	27.64	33.83	37.9	18.67	32.33	3.87		
Fe ₂ O ₃	1.11	2.37	2.2	2.4	1.69	2.49	6.77	3.69	2.57	1.77	3.06	5.91	2.26	2.14	23.49	5.54	4.22	2.83	2.26	3.94	21.49	13.63	1.31	36.91	11.77	9.97			
SiO ₂	1.78	24.24	7.21	19.07	2.05	21.79	1.97	1.56	11.99	2.34	11.97	18.92	12.62	8.92	21.32	24.4	15.76	12.23	30.36	30.79	4.38	37.87	37	41.2	21.35	28.99	4.37		
TiO ₂	4.23	1.92	3.96	3.5	5.11	5.3	3.98	3.06	5.15	3.03	2.58	2.32	4.34	2.6	2.2	3.22	3.56	2.2	2.48	0.94	1.66	2.09	3.04	1.29	1.96	/	0.39		
P ₂ O ₅	0.63	/	0.63	0.10	0.31	/	0.89	0.61	0.36	0.66	0.22	/	0.30	1.15	/	/	0.52	/	/	/	/	/	/	/	/	/			
Ba	32.6	46.2	72.4	131	18.4	147	54.1	35	94.4	37.8	105	178	75.4	280	34.2	37.9	65.4	84.99	112	27.2	130	292	61.9	77.6	37.3	105.4	144.5		
Cr	140	230	130	290	160	370	170	140	120	160	130	120	160	130	130	120	120	220	40	110	90	120	120	120	120	120	20		
Cs	0.4	1.33	0.64	2.13	0.59	2.31	0.49	0.28	1.74	0.59	1.85	1.5	1.61	1.51	1.35	1.69	1.65	1.22	2.28	1.2	0.74	6.62	1.34	1.6	0.76	2.08	1.17		
Hf	25.7	12	37.8	36.1	32.6	121.5	27.6	26	31.3	29.7	31.5	26	30.9	36.6	32.9	29.4	22.8	34.73	20.3	13.6	5.2	19.3	18.8	9.9	19.5	15.23	3.3		
Nb	96.1	48.7	85.3	85.5	79.5	113.5	118.5	93.4	68.7	118.5	67	56	57	91.3	58.1	51.7	73.8	80.15	45.5	57.1	19.4	33.9	47.1	25.7	69.3	42.57	7.3		
Rb	3	9.9	20.7	43.1	3.2	9.1	4.8	2.2	34.3	6.4	37	53.8	35.3	26.2	5.2	6.6	19.7	18.85	25.4	4.8	12.3	122.5	11.7	13.3	6.4	28.06	13.3		
Sn	26	14	26	54	20	17	28	26	18	32	21	18	16	26	14	13	20	22.88	359	15	16	10	14	6	17	62.43	27		
Sr	98.5	175.5	86.6	220	413	158.5	147.5	119.0	471	950	285	131.5	642	2000	1180	898	640	745.3	431	437	268	1150	539	317	1525	666.7	87.9		
Ta	7.5	3.8	6.4	6.1	8.5	9.2	7.2	5.2	9	5.4	4.4	4.4	4.4	7	4.3	3.8	5.5	6.12	3.4	4.2	1.5	2.5	3.6	2.1	5.2	3.21	0.6		
Th	1.34	81.9	106.5	72.3	93.9	62.8	178.5	124.5	76	179.5	75.1	42.1	59.3	143	56.2	50.3	93.1	95.82	60.2	68.9	27.3	46.3	65.4	37.1	99.6	57.83	8.11		
U	46.8	20.9	32.8	35.3	35.9	32.2	58.4	39.4	26.4	62.4	49.5	18.9	18	43.2	21.2	24	31.5	35.11	18.25	18.9	9.56	12.8	19.85	23.8	25.3	18.35	3.35		
V	248	354	187	182	163	159	159	279	167	207	133	136	297	233	118	151	289	249	183	81	326	182	204	191	202.3	30			
W	13	20	13	14	13	18	17	17	12	16	12	10	14	12	12	10	13.71	110	10	88	6	6	9	19.29	4				
Zr	83.6	380	1240	1210	1090	4130	887	847	1050	997	1050	870	1040	1210	1110	996	737	1158	680	447	179	669	620	335	667	513.9	113		
Y	123	51	173	83.6	146.5	167.5	201	164.5	163.5	153	115.5	86.4	95.3	449	63.8	59.8	166.5	144.88	79.2	46.8	26.7	57.3	254	256	66.5	112.4	18.1		
La	57.2	134	231	57.6	286	41.6	51.7	304	181.5	494	186	89.5	151.5	361	86.5	96.2	223	256.02	182	144	81.1	92.6	155	81.4	229	137.9	13.2		
Ce	96.0	202	442	101.5	498	80.2	83.3	53.0	406	858	410	168	307	719	265	232	427	437.57	399	277	128.5	178	285	170	373	258.6	24.3		
Pr	118.5	28.1	58.7	12.2	56.7	8.61	120.5	70.6	40.1	115.5	37.1	17.8	31.7	98.4	17.65	21	54.9	53.42	56.8	23.9	21.1	20.7	44.2	18.7	60.6	35.14	3.12		
Nd	369	91.4	235	42.9	182.5	32.2	41.5	25.1	135.5	393	117	55.3	99.7	394	55	62.5	212	184.9	242	66.7	81.4	83.1	210	72	232	141.03	12.2		
Sm	62.1	15.5	44.8	8.16	28.6	10.1	70.1	45.9	58	18.85	9.18	17.65	10.55	9.2	10	49.8	34.54	40.6	8.74	12.59	19.7	63.3	21.7	28.8	27.91	2.52			
Eu	8.75	2.39	8.49	1.67	4.86	3.26	12.65	7.88	4.89	9.55	3.36	1.62	3.51	19.65	1.82	8.74	6.17	7.32	1.67	1.99	3.82	12.9	6.81	4.54	5.58	0.54			
Gd	31.5	10.8	36.3	9.2	24.7	18.95	47.9	33.6	24.7	36.6	17.85	10.7	17.95	9.17	8.67	8.18	34.3	27.27	24.9	7.84	7.31	12.45	61.1	37.6	17.6	24.11	3.205		
Tb	4.12	1.68	5.48	4.47	3.62	6.51	5.17	4.41	5.09	3.34	2.15	3.01	15.75	1.63	1.4	5.33	4.42	2.89	1.38	0.94	1.8	9.81	6.23	2.34	3.63	0.53			
Dy	23.7	9.92	31.4	13.5	27.4	24.5	36.6	30.6	26.2	29.5	20.7	14.25	18.25	91.2	10.35	9.56	31.3	26.41	15.45	8.94	5.29	10.5	55.5	35.8	13.35	20.69	3		
Ho	4.83	2.1	6.55	3.07	5.47	5.44	7.34	6.19	4.34	6.28	5.63	6.19	4.34	3.69	5.06	2.26	2.23	6.24	5.46	3.01	1.96	1.01	2.23	1.08	7.19	2.76	4.14	0.63	
Er	14.1	5.92	18.9	8.88	14.8	15.95	20.6	17.3	15.45	17.5	12.1	8.58	10.5	48.5	6.71	7.65	7.15	15.28	8.69	5.82	2.75	6.56	27.8	18.6	8.43	11.24			
Tm	2.23	0.93	3	1.37	2.19	2.57	3.18	2.69	2.1	2.76	1.75	1.33	1.56	7.08	1.04	1.09	2.51	2.32	1.34	0.96	0.42	1.11	3.89	2.45	1.45	1.66	0.25		
Yb	14.9	5.73	18.35	9.2	13.75	16.45	19.7	16.95	12.75	17.7	11.05	8.35	10.35	42.1	7.12	7.48	15.4	14.55	8.67	6.13	2.76	7.75	13.7	10.2	10.39	1.56			
Lu	2.4	0.93	2.77	1.44	2.06	2.81	3.15	2.66	1.96	2.81	1.71	1.32	1.64	6.15	1.13	1.18	2.53	2.27	1.39	0.99	0.42	1.21	3.61	2.16	1.68	1.64	0.26		
ΣREE	218.8	511.4	1143	272.6	1152	266.3	2113	1325	884.9	2046	845.2	391.1	678.2	2018	474.1	161.4	1090	994.1	556	347.5	441.5	966.4	494.2	985.8	683.6	67			
(La/Yb) _N	0.77	0.69	0.79	0.80	0.82	0.75	0.99	0.75	0.93	0.78	0.92	0.80	1.41	1.08	0.80	0.87	0.82	0.98	0.65	0.85	0.72	0.91	0.66	0.80	0.79				
Eu/Eu*	0.67	0.63	0.72	0.66	0.62	0.80	0.74	0.68	0.69	0.71	0.62	0.56	0.67	0.68	0.70	0.72	0.68	0.79	0.69	0.83	0.71	0.81	0.69	0.75	0.65				
(La/Sm) _N	5.76	5.40	3.22	4.41	6.25	2.57	4.61	4.14	4.79	5.32	6.17	6.09	5.36	2.14	5.88	6.01	4.76	2.80	10.30	4.04	2.94	1.53	2.34	4.97	4.13	3.27			
(Gd/Yb) _N	1.30	1.16	1.21	0.61	1.10	0.71	1.49	1.21	1.19	1.27	0.99	0.79	1.06	1.33	0.75	0.67	1.37	1.07	1.76	0.78	1.62	0.98	1.59	1.68	1.36	1.26			
ΣREE/ΣHREE	21.38	12.45	8.31	4.61	11.14	1.95	13.58	10.49	8.49	16.32	10.60	6.86	9.13	5.30	11.18	8.49	9.72	13.98	15.34	15.63	9.12	3.93	3.00	16.05	7.82	5.02			
TiO ₂ /Al ₂ O ₃	0.058	0.035	0.057	0.070	0.048	0.097	0.079	0.057	0.047	0.071	0.047	0.047	0.037	0.066	0.050	0.043	0.055	0.057	0.049	0.073	0.060	0.062	0.080	0.069	0.063	0.054			

$\Sigma\text{REE} = \text{ΣREE(La-Lu)}; \Sigma\text{REE} = \Sigma\text{REE(Gd-Lu)}(\text{La/Yb})\text{N}; \text{Eu/Eu}^* = (\text{Eu}/\text{Eu}_{\text{Ch}})\times\left(\frac{\text{Sm}}{\text{Sm}_{\text{Ch}}}\right)\times\left(\frac{\text{Gd}}{\text{Gd}_{\text{Ch}}}\right); \text{Eu}_{\text{Ch}}, \text{Sm}_{\text{Ch}}, \text{Gd}_{\text{Ch}}$ for normalization of chondrite, Normalization factors are from Anders and Grevesse (1989).

Table 4

Correlation coefficients (Pearson's r) between chemical compositions of bauxite ores from the Yunfeng deposit, central Guizhou Province.

	Al ₂ O ₃	Fe ₂ O ₃	SiO ₂	TiO ₂	Cr	Hf	Nb	Ta	Th	U	Zr	Y	LREE	HREE
Al ₂ O ₃	1.00													
Fe ₂ O ₃	-0.41	1.00												
SiO ₂	-0.97	0.28	1.00											
TiO ₂	0.49	-0.21	-0.59	1.00										
Cr	0.13	-0.07	-0.20	0.35	1.00									
Hf	-0.26	-0.07	0.22	0.44	-0.09	1.00								
Nb	0.52	-0.23	-0.61	0.99	0.37	0.42	1.00							
Ta	0.55	-0.24	-0.64	0.99	0.39	0.39	1.00	1.00						
Th	0.73	-0.21	-0.78	0.74	0.38	-0.19	0.77	0.79	1.00					
U	0.66	-0.25	-0.71	0.79	0.36	-0.01	0.80	0.83	0.86	1.00				
Zr	-0.27	-0.06	0.23	0.43	-0.09	1.00	0.41	0.38	-0.20	-0.02	1.00			
Y	0.40	-0.22	-0.43	0.53	-0.05	0.16	0.48	0.49	0.55	0.42	0.15	1.00		
LREE	0.80	-0.20	-0.84	0.60	0.17	-0.30	0.63	0.65	0.93	0.79	-0.31	0.53	1.00	
HREE	0.46	-0.22	-0.49	0.53	-0.03	0.06	0.49	0.50	0.63	0.47	0.05	0.99	0.62	1.00

source of carbonate and igneous rocks (Mongelli et al., 2014; Liu et al., 2017).

As introduced earlier, the paleo-karstic bauxite deposits in central Guizhou Province have been generally thought to be derived from weathering of carbonate rocks that underlie the deposits (i.e., autochthonous origin), including the Middle to Upper Cambrian Loushanguan Group dolomite for most of the deposits in the region (Li et al., 2014; Liu and Liao, 2014), Middle Cambrian Shilengshui Formation dolomite for the Lindai deposit (Ling et al., 2013, 2017), and Lower Cambrian Qingxudong Formation dolomite for the Heitudian deposit (Yang et al., 2014). However, the possibility of other rocks below the sub-Carboniferous unconformity as potential source rocks cannot be discounted (Yang et al., 2014). The potential source rocks include, in addition to the carbonates mentioned above, dolomite of the Sinian Dengying Formation, the “Black Rock Sequence” of the Lower Cambrian Niutitang Formation, and siliciclastic rocks with intercalated limestone of the Lower Cambrian Mingxinsi and Jindingshan formations (Fig. 2a). Furthermore, Ordovician strata are locally preserved in the Qianzhong Uplift, including the Meitan and Tongzi formations that contain thick shale layers, and these rocks can also be potential source rocks for the bauxite deposits. Based on the major, trace and rare earth element data of the Yunfeng bauxite deposit as documented in this paper, we think the bauxite ores in this area were mainly derived from two source rocks, i.e., dolomite of the Loushanguan Group underlying the deposit (autochthonous source) and “Black Rock Sequence” of the Niutitang Formation (allochthonous source). Although the latter source rock was not exposed in the immediate surrounding areas of the Yunfeng deposit in Early Carboniferous, it was exposed to the west of the study area, at the core of the anticline in the central part of the Qianzhong Uplift (Fig. 1b). The sub-rounded shape of some of the bauxite clasts (Fig. 3f and g) supports the notion that they were transported from a distal (allochthonous) source. The geochemical reasoning for the mixed autochthonous and allochthonous sources for the Yunfeng bauxite is discussed below.

Immobile elements such as Al, Ti, Th, Nb and Ta, especially their ratios, have been widely used to constrain the provenances of karstic bauxite deposits (Mongelli, 1997; Mameli et al., 2007; Liu et al., 2013; Gu et al., 2013; Zamanian et al., 2016; Ahmadnejad et al., 2017; Liu et al., 2017). The observation that the Al₂O₃ vs TiO₂, TiO₂ vs Th, Th vs Nb, Ta vs Th and Nb vs Ta binary diagrams show good linear correlations for the bauxite ores and bauxitic clays, and the linear correlations extend to the Loushanguan dolomite and its weathering products as well as the “Black Rock Sequence” (Fig. 7a, d and e, and Fig. 8a, c and d), suggest that both the dolomite and “Black Rock Sequence” may be the source rocks. The TiO₂ /Al₂O₃ ratios, which are generally considered to be inherited from the protoliths (Mameli et al., 2007; Mongelli et al., 2014; Hou et al., 2017; Ahmadnejad et al., 2017), range from 0.035 to 0.097 for the bauxite ores and 0.049 to 0.08 for the

bauxitic clays; these ratios are close to those of the “Black Rock Sequence” (0.04 to 0.071 for samples from Kaiyang in central Guizhou (data from Zhang et al., 2016) and the Loushanguan dolomite and its weathering products (0.20–0.214; data from Ji et al., 1999) (Table 3, Fig. 10a).

Rare earth elements are generally regarded as an excellent instrument for tracing the sources of weathered materials (Esmaeily et al., 2010; Gu et al., 2013; Zamanian et al., 2016; Ahmadnejad et al., 2017; Liu et al., 2013, 2017). The normalized REE distribution pattern of the weathering products mostly inherited certain particular geochemical characteristics of their parent materials, and the Eu anomaly was considered to retain during intense weathering and was utilized for identifying the provenance rocks of bauxite (Mameli et al., 2007; Liu et al., 2013). In this study, the Eu anomalies of the bauxite ores and bauxitic clays are generally similar to those of the Loushanguan dolomite and its weathering products as well as the “Black Rock Sequence” (Figs. 9 and 10). In the Eu/Eu* vs TiO₂/Al₂O₃ binary diagram, the bauxite ores, bauxite clays, “Black Rock Sequence” and Loushanguan dolomite and its weathering products plot close to each other and to the average composition of upper crustal rocks, and are far from granite or basalt (Fig. 10a). Like Eu/Eu* ratio, the Sm/Nd ratio is also considered to reflect the source rocks of bauxite as only minor fractionation of Sm and Nd occurs during intense chemical and biological weathering (Viers and Wasserburg, 2004; Ahmadnejad et al., 2017). In the Eu/Eu* vs Sm/Nd diagram, which is commonly used to trace the provenance of weathered materials (Mongelli et al., 2014; Ahmadnejad et al., 2017), the majority of bauxite ores, bauxitic clays, “Black Rock Sequence” and Loushanguan dolomite and its weathering products plot close to each other and to the Post-Archean Australian Shales (PAAS) and Cratonic sandstones, but far away from andesite and felsic volcanic rocks (Fig. 10b). The overall similar REE patterns of the bauxite ores, bauxitic clays, “Black Rock Sequence” and Loushanguan dolomite and its weathering products, except for the relatively high total REE contents in the bauxite ores (Fig. 9), which is possibly due to enrichment of REE in accessory minerals, also support the notion that the bauxite was derived from either the “Black Rock Sequence” or the Loushanguan dolomite, or a mixture of both.

Although either the Loushanguan dolomite or the “Black Rock Sequence” could explain the immobile elements and rare earth elements characteristics of the bauxite ores, the dolomite alone cannot explain the high U and Th concentrations in the ores, as discussed below. It is well known that certain bauxite ores contain significantly greater amounts of Th and U than the average crustal rocks (Richardson, 1959; Huang et al., 2014). Richardson (1959) indicated that a relationship exists between the type of rock from which a bauxite is derived and the Th and U contents in the bauxite, and Lukas et al. (1983) suggested that the Th and U values could furnish a suitable method for differentiating allochthonous bauxites from those formed in

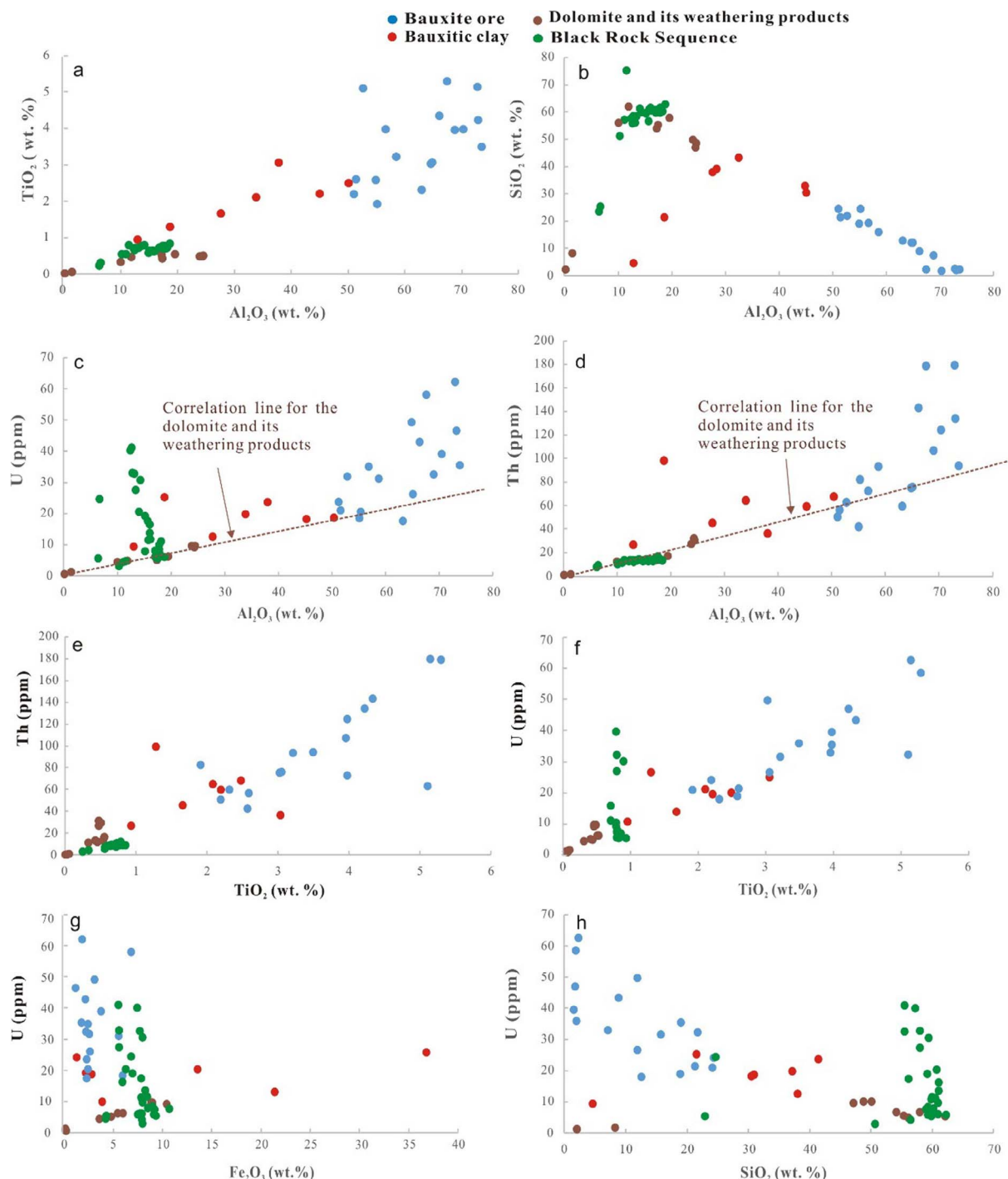


Fig. 7. Binary diagrams for selected elements showing correlations between: (a) TiO_2 vs Al_2O_3 ; (b) SiO_2 vs Al_2O_3 ; (c) U vs Al_2O_3 ; (d) Th vs Al_2O_3 ; (e) Th vs TiO_2 ; (f) U vs TiO_2 ; (g) U vs Fe_2O_3 and (h) U vs SiO_2 in bauxite ores, bauxitic clays, dolomite and its weathering products of the Loushanguan Group, Xinpu, Zunyi, Guizhou (data from Ji et al., 1999) and the “Black Rock Sequence”, Kaiyang, Guizhou (data from Zhang et al., 2016). (For interpretation of the references to colour in this figure legend, the reader is referred to the web version of this article.)

situ. Despite the fact that U is generally not an immobile element during weathering processes, a linear correlation between Al_2O_3 and U was found in some bauxite ores (Richardson, 1959). Such a linear correlation between Al_2O_3 and U is also found for a paleo-weathering profile of the Loushanguan dolomite in Zunyi (Fig. 2c) (Fig. 7c, data from Ji et al., 1999). This linear correlation is probably due to U absorption in Fe oxides, as reflected by the positive linear correlation between U and Fe_2O_3 (Fig. 7g), during the weathering of dolomite. If the bauxite ores and bauxitic clays are derived from the weathering of the Loushanguan dolomite, their U and Al_2O_3 data would fall on the regression line for

the Loushanguan dolomite and its weathering products (Fig. 7c). However, contrary to this prediction, the majority of the bauxite ores and bauxitic clays plot above the dolomite line (Fig. 7c), indicating that the weathering of the Loushanguan dolomite alone cannot produce the bauxite ores with high U concentrations, and other source rocks must have been involved.

The most likely source for U for the Yunfeng bauxite, is the “Black Rock Sequence”. It is well known that the “Black Rock Sequence”, which is widely developed in South China, is rich in P, Ni, Sb, Cu, Zn, Pb, REE and U (Zhou et al., 2008; Deng et al., 2010a,b; Li et al., 2013;

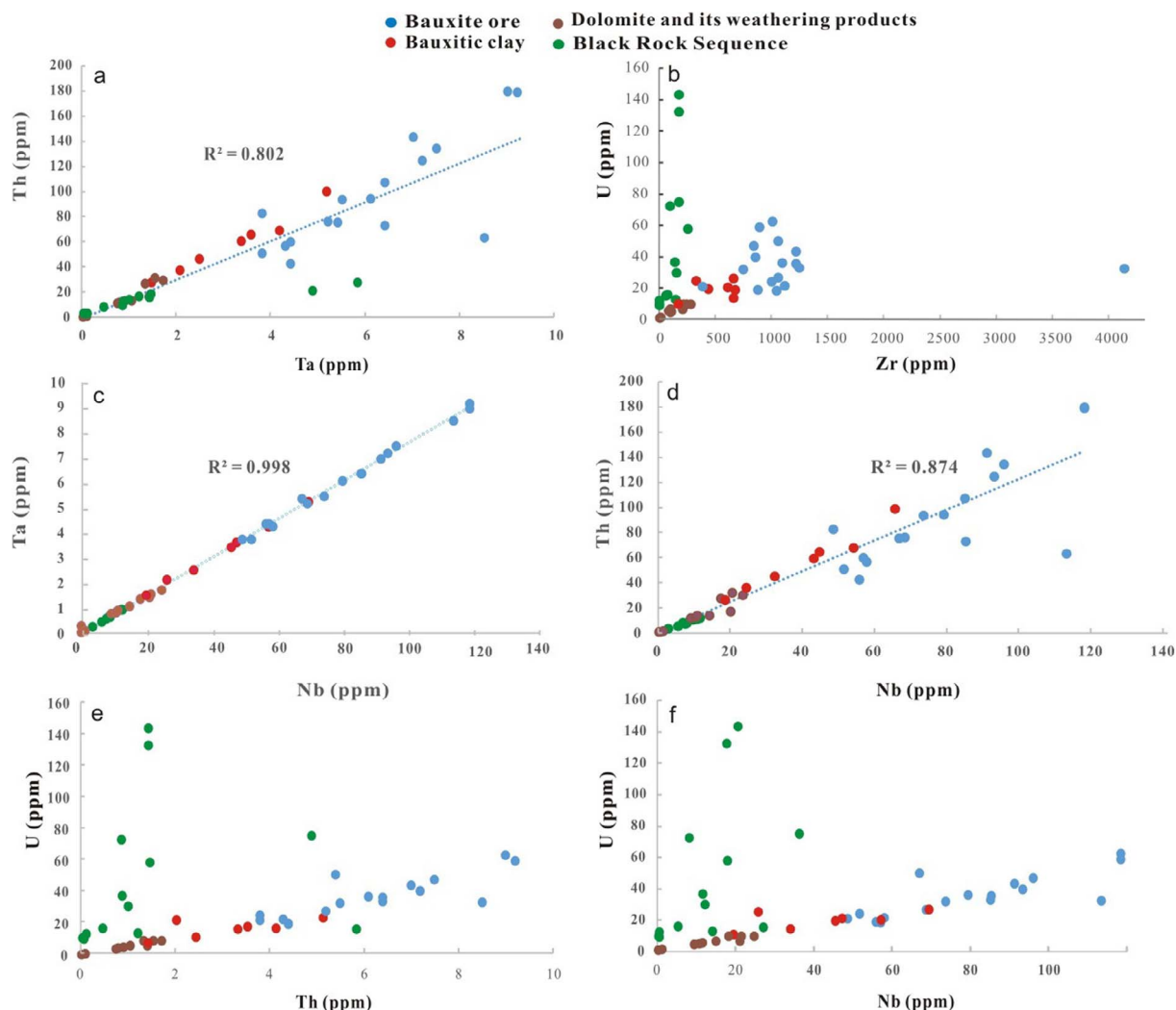


Fig. 8. Plots of (a) Ta vs Th, (b) Zr vs U, (c) Nb vs Ta, (d) Nb vs Th, (e) U vs Th and (f) U vs Nb for bauxite ores, bauxitic clays, dolomite and its weathering products of the Loushanguan Group, Xinpu, Zunyi, Guizhou (data from Ji et al., 1999) and the Lower Cambrian Niutitang Formation “Black Rock Sequence”, Zhenyuan, Guizhou (Data from Yang et al., 2013).

(Yang et al., 2013; Pi et al., 2013; Zhao et al., 2014; Zhang et al., 2016). The average U content of the “Black Rock Sequence” in Guizhou Province is 40.77 ppm (Yang et al., 2013), and many uranium minerals (e.g. pitchblende, coffinite, and brannerite), uranium deposits and Ni-Mo-PGE deposits have been found in this stratigraphic interval in South China (Mao et al., 2001; Qi et al., 2014; Zhao et al., 2014; Pi et al., 2013; Wang, 2015). As noted above, the U and P contents in the Yunfeng bauxite are fairly high, and various minerals containing the trace elements including stibnite, cobalt–nickel-bearing arsenopyrite, cobalt-bearing pentlandite, xenotime, chalcopyrite, galena and U-bearing mineral were observed in the bauxite ores.

Nevertheless, the enrichment of U in the bauxite ores cannot be explained simply by in situ weathering of the “Black Rock Sequence”. As shown in Fig. 7f and Fig. 8e and f, the bauxite ores have comparable U contents as the “Black Rock Sequence”; if the bauxite was derived from in situ weathering of the “Black Rock Sequence”, and all the U was retained, then much higher U contents would have been produced in the bauxite ores. It is important to note that U may be oxidized to U^{6+} during the weathering processes, which may be partly dissolved in water and leached, and partly adsorbed on Fe- and Al-oxides and hydroxides (Richardson, 1959; Cumberland et al., 2016). Therefore, although the “Black Rock Sequence” most likely contributed to the formation of the Yunfeng bauxite ores, U is not significantly enriched (Fig. 7c, Fig. 8 e and f). In contrast, Th is generally immobile under supergene conditions and most of the Th minerals can resist weathering

and remain in their original forms (Richardson, 1959; Adams and Richardson, 1960; Lukas et al., 1983; Pollack et al., 2009). As a result, Th was significantly enriched in the bauxite ores relative to both the dolomite and the “Black Rock Sequence” (Fig. 7d). The transport and accumulation of U, as a mobile element both in weathering and diagenetic processes, needs further examination in future studies, especially considering that the paleo-karstic bauxite deposits were subject to variable degrees of diagenesis, which may have been important in bauxite formation (Merino and Banerjee, 2008).

6. Conclusions

- (1) The bauxite orebodies in the Xiuwen-Qingzhen area occur as lenticular and stratiform shapes lying unconformably above dolomite of the Middle-Upper Cambrian Loushanguan Group. The bauxite ores contain sub-rounded to well-rounded grains of residual minerals and rock clasts indicating transport over significance distance.
- (2) The bauxite ores are characterized by relatively high levels of P and U. In addition to the common minerals of diaspore, kaolinite, hematite, anatase, chamosite, chlorite, pyrite, zircon and rutile, the Yunfeng bauxite ores also contain trace amounts of galena, chalcopyrite, stibnite, xenotime, uranium-bearing minerals, cobalt- and nickel-bearing arsenopyrite and cobalt-bearing pentlandite.
- (3) The REE patterns, the correlations between Al_2O_3 vs TiO_2 , TiO_2 vs

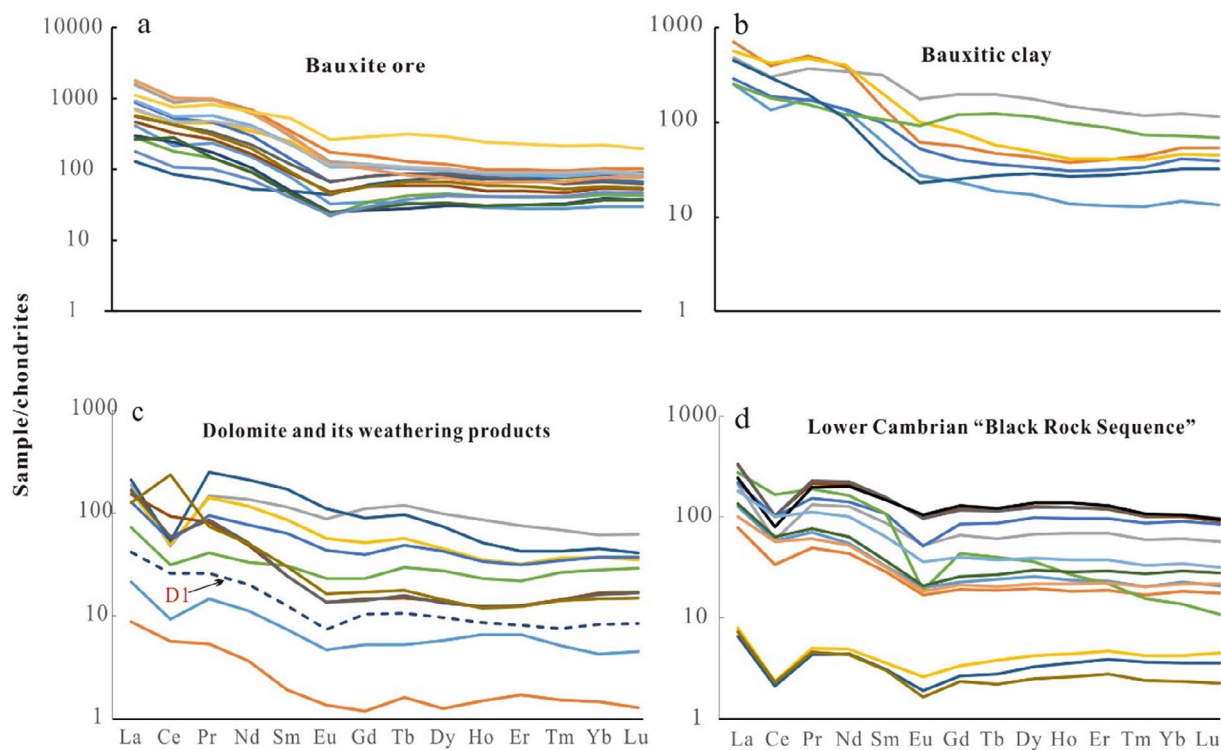


Fig. 9. Chondrite-normalized REE patterns of bauxite ores, bauxitic clays, semi-weathered dolomite from the Qinzheng area, dolomite and its weathering products of the Loushanguan Group (data from Ji et al., 1999) and the Lower Cambrian “Black Rock Sequence” (data from Yang et al., 2013). Normalization factors are from Anders and Grevesse (1989).

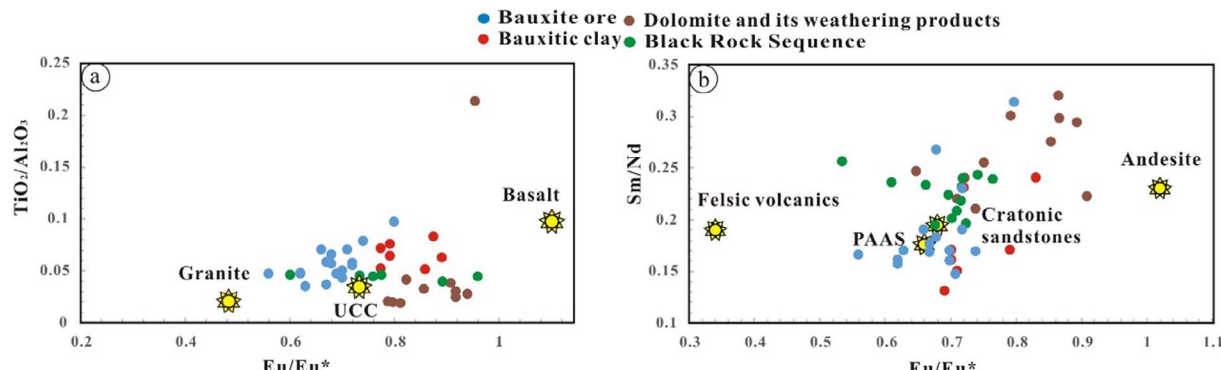


Fig. 10. Binary diagrams (a) Eu/Eu^* and $\text{TiO}_2/\text{Al}_2\text{O}_3$, (b) Eu/Eu^* vs Sm/Nd for bauxite ores, bauxitic clays, dolomite and its weathering products of the Loushanguan Group (data from Ji et al., 1999) and the Lower Cambrian Niutitang Formation “Black Rock Sequence”, Zhipin, Guizhou (data from Wang and Zhang, 2016); (b) binary diagram for bauxite ores, bauxitic clays, dolomite and its weathering products of the Loushanguan Group, Xinpu, Zunyi, Guizhou (data from Ji et al., 1999) and the Lower Cambrian Niutitang Formation “Black Rock Sequence”, Zhenyuna, Guizhou (data from Yang et al., 2013). Granite and basalt from Ahmadnejad et al. (2017); Upper continental crust rocks (UCC), Cratonic sandstones and Felsic volcanics from Taylor and McLennan (1985); Andesite and Post-Archean Australian Shales (PAAS) from Condie (1993).

Th, Th vs Nb, Ta vs Th and Nb vs Ta as well as plots of Eu/Eu^* vs $\text{TiO}_2/\text{Al}_2\text{O}_3$ and Eu/Eu^* vs Sm/Nd of the bauxite ores and bauxitic clays suggest that the bauxite was derived from dolomite of the Middle-Upper Cambrian Loushanguan Group or the “Black Rock Sequence” of Lower Cambrian Niutitang Formation. However, the elevated concentrations of U, Th, P, Co, Ni and Sb in the bauxite ores cannot be explained by in situ weathering of dolomite alone. It is inferred that the bauxite ores in the Yunfeng bauxite are mixtures of bauxite from in situ weathering of dolomite and transported bauxite derived from weathering of the underlying strata which were exposed in areas distal from Yunfeng, especially for the “Black Rock Sequence” of Low Cambrian Niutitang Formation. Thus, the Yunfeng bauxite ores, and by inference many other paleo-karstic bauxite deposits in central Guizhou Province, are of mixed autochthonous and allochthonous origin.

Acknowledgments

We appreciate Yang, J. C. and Dr. Yang, W. for assistance in the field work, and Prof. Gu, X.P. for discussion and suggestions during this study. This work was jointly supported by Qingzhen Yunfeng Aluminum and Iron Mining Co. (738010033), the Innovation-driven Plan in Central South University (Grant 2015CX008).

References

- Anders, E., Grevesse, N., 1989. *Geochim. Cosmochim. Acta* 53, 197.
- Adams, J.A.S., Richardson, K.A., 1960. Thorium, uranium and zirconium concentrations in bauxite. *Econ. Geol.* 55 (8), 1653–1675.
- Ahmadinejad, F., Zamanian, H., Taghipour, B., Zarasvandi, A., Buccione, R., Ellahi, S.S., 2017. Mineralogical and geochemical evolution of the Bidgol bauxite deposit, Zagros Mountain Belt, Iran: implications for ore genesis, rare earth elements fractionation and parental affinity. *Ore Geol. Rev.* 86, 755–783.
- Bárdossy, G., Aleva, G.J., 1990. Lateritic Bauxites. Elsevier Scientific Publication,

- Amsterdam, pp. 1–624.
- Bárdossy, G., 1982. Karst Bauxites. Elsevier, Amsterdam pp. 441.
- Bogatyrev, B., Zhukov, V., Tsekhevsky, Y.G., 2009. Formation conditions and regularities of the distribution of large and superlarge bauxite deposits. *Lithol. Miner. Resour.* 44, 135–151.
- Combes, P.J., Oggiano, G., Temussi, I., 1993. Geodynamique des bauxites sardes, typologie, génèse et contrôle paleotectonique. *Comptes Rendus de l'Académie des Sciences Série II* 316, 403–409.
- Condie, K.C., 1993. Chemical composition and evolution of the upper continental crust: contrasting results from surface samples and shales. *Chem. Geol.* 104, 1–37.
- Cumberland, S.A., Douglas, G., Grice, K., Moreau, J.W., 2016. Uranium mobility in organic matter-rich sediments: A review of geological and geochemical processes. *Earth-Sci. Rev.* 159, 160–185.
- Deng, J., Wang, Q.F., Yang, S.J., Liu, X.F., Zhang, Q.Z., Yang, L.Q., Yang, Y.H., 2010a. Genetic relationship between the Emeishan plume and the bauxite deposits in western Guangxi, China: constraints from U-Pb and Lu-Hf isotopes of the detrital zircons in bauxite ores. *J. Asian Earth Sci.* 37 (5–6), 412–424.
- Deng, X., Yang, K.G., Liu, Y.L., She, Z.B., 2010b. Characteristics and tectonic evolution of Qianzhong Uplift. *Earth Sci. Front.* 17 (3), 79–89 (In Chinese with English abstract).
- Dill, H.G., 2017. Residual clay deposits on basement rocks: The impact of climate and the geological setting on supergene argillitization in the Bohemian Massif (Central Europe) and across the globe. *Earth Sci. Rev.* 165, 1–58.
- Esmaeily, D., Rahimpour-Bonab, H., Esna-Ashari, A., Kananian, A., 2010. Petrography and geochemistry of the Jajarm Karst bauxite ore deposit, NE Iran: implications for source rock material and ore genesis. *Turk. J. Earth Sci.* 19, 267–284.
- Gao, D., Sheng, Z., Shi, S., Chen, L., 1992. Studies on the Bauxite Deposit in Central Guizhou, China. Guizhou Science & Technology Publishing House, Guiyang pp. 11–20 (in Chinese).
- Gu, J., Huang, Z.L., Fan, H.P., Jin, Z.G., Yan, Z.F., Zhang, J.W., 2013. Mineralogy, geochemistry, and genesis of lateritic bauxite deposits in the Wuchuan-Zheng'an-Daozhen area, northern Guizhou Province. *J. Geochem. Explor.* 130, 44–59.
- Guizhou Bureau of Geology and Minerals, 1987. Geological Marks of Guizhou Province. Geological Publishing House, Beijing pp. 1–360 (in Chinese).
- Hanilçi, N., 2013. Geological and geochemical evolution of the Bolkardağı bauxite deposits, Karaman, Turkey: Transformation from shale to bauxite. *J. Geochem. Explor.* 133, 118–137.
- Hou, Y., Zhang, Y., Xu, Y., He, B., 2017. The provenance of late Permian karstic bauxite deposits in SW China, constrained by the geochemistry of interbedded clastic rocks, and U-Pb-Hf-O isotopes of detrital zircons. *Lithos* 278–281, 240–254.
- Huang, Z.L., Jin, Z.G., Xiang, X.L., Gu, J., Wu, G.H., Chen, X.L., Su, Z.L., Zho, Y.Y., Zuo, Y.L., 2014. Metallogenetic Theory and prediction of bauxite deposits in the Wuchuan-Zheng'an-Daozhen area, Northern Guizhou province, China. Science Press pp. 89–99.
- Ji, H.B., Ouyang, Z.Y., Wang, S.J., Zhoi, D.Q., 1999. Element geochemical characteristics of the dolomite weathering profile and its significance to the upper continental crust average chemical composition, as Xin Pu profile, North Guizhou for an example. *Sci. China (D)* 29, 504–513 (in Chinese).
- Li, J., Yu, B.S., Guo, F., 2013. Depositional setting and tectonic background analysis on Lower Cambrian black shales in the North of Guizhou Province. *Acta Sedimentol. Sin.* 31 (1), 20–31 (in Chinese with English abstract).
- Li, Y.T., Xiao, J.F., Fu, S.H., Zhao, Z.J., 2014. The comparison study on metallogenetic characteristics of the main bauxite-deposit-clustered areas in Guizhou province. *Contribut. Geol. Miner. Resour. Res.* 4, 489–494 (in Chinese with English abstract).
- Ling, K.Y., Zhu, X.Q., Wang, Z.G., Han, T., Tang, H.S., 2013. Metallogenetic model of bauxite in Central Guizhou Province: an example of Lindai deposit. *Acta Geol. Sin. (Engl. Ed.)* 87 (6), 1630–1642.
- Ling, K.Y., Zhu, X.Q., Tang, H.S., Wang, Z.G., Yan, H.W., Han, T., Chen, W.Y., 2015. Mineralogical characteristics of the karstic bauxite deposits in the Xiuhu ore belt, Central Guizhou Province, Southwest China. *Ore Geol. Rev.* 65, 86–96.
- Ling, K.Y., Zhu, X.Q., Tang, H.S., Li, S.X., 2017. Importance of hydrogeological conditions during formation of the karstic bauxite deposits, Central Guizhou Province, Southwest China: a case study at Lindai deposit. *Ore Geol. Rev.* 82, 198–216.
- Liu, P., 2001. Discussion on the metallogenetic setting of the Qianzhong-Yu'an bauxite in Guizhou and its genesis. *Guizhou Geol.* 18 (4), 238–243 (In Chinese with English abstract).
- Liu, X., Wang, Q., Feng, Y., Li, Z., Cai, S., 2013. Genesis of the Guangou karstic bauxite deposit in western Henan. *Ore Geol. Rev.* 55, 162–175.
- Liu, P., Liao, Y.H., 2014. Regional metallogenetic model and prospecting criteria of sedimentary bauxite deposits in Central Guizhou—Southern Chongqing region. *Geol. China* 41 (6), 2063–2082 (in Chinese with English abstract).
- Liu, P., Liao, Y.C., Zhang, Y.J., 2015. Characteristics of marine deposits of the bauxite-bearing rock series in central Guizhou-Southern Chongqing area. *Guizhou Geol.* 42 (2), 641–654 (in Chinese with English abstract).
- Liu, X., Wang, Q., Zhang, Q., Yang, S., Liang, Y., Zhang, Y., Li, Y., Guan, T., 2017. Genesis of the Permian karstic Pingguo bauxite deposit, western Guangxi, China. *Miner. Deposita*. <http://dx.doi.org/10.1007/s00126-017-0723-y>.
- Lukas, T.C., Loughan, F.C., Eades, J.L., 1983. Origin of bauxite at Eufaula, Alabama, USA. *Clay Miner.* 18, 127–138.
- MacLean, W., Bonavia, F., Sanna, G., 1997. Argillite debris converted to bauxite during karst weathering: evidence from immobile element geochemistry at the Olmedo Deposit, Sardinia. *Mineral. Deposita* 32, 607–616.
- Mameli, P., Mongelli, G., Oggiano, G., Dinelli, E., 2007. Geological, geochemical and mineralogical features of some bauxite deposits from Nurra (Western Sardinia, Italy): insights on conditions of formation and parental affinity. *Int. J. Earth Sci.* 96, 887–902.
- Mao, J.W., Zhang, G.D., Du, A.D., Wang, Y.T., Zeng, M.G., 2001. Geology, geochemistry, and Re-Os isotopic dating of the Huangjiawan Ni-Mo-PGE deposit, Zunyi, Guizhou province. *ACTA Geol. Sin.* 75 (2), 234–243 (In Chinese with English abstract).
- Mei, M.X., Zhao, H., Meng, X.Q., Chen, Y.H., 2006. Sequence-stratigraphic framework and its forming background of alaeogeography for the middle Cambrian of the Upper Yangtze region. *Geol. J. China Univ.* 12 (3), 328–342 (In Chinese with English abstract).
- Merino, E., Banerjee, A., 2008. Terra rossa genesis, implications for karst, and eolian dust: a geodynamic thread. *J. Geol.* 116, 62–75.
- Mongelli, G., 1997. Ce anomalies in the textual components of upper Cretaceous karst bauxites from the Apulian carbonate platform (southern Italy). *Chem. Geol.* 140, 69–79.
- Mongelli, G., Boni, M., Buccione, R., Sinisi, R., 2014. Geochemistry of the Apulian karst bauxites (southern Italy): chemical fractionation and parental affinities. *Ore Geol. Rev.* 63, 9–21.
- Mutakayawa, M.K.D., Ikingura, J.R., Mruma, A.H., 2003. Geology and geochemistry of bauxite deposits in Lushoto District, Usambara Mountains, Tanzania. *J. Afr. Earth Sci.* 36, 357–369.
- Özlü, N., 1983. Trace element contents of karst bauxites and their parent rocks in the Mediterranean belt. *Mineral. Deposita* 18, 469–476.
- Pi, D.H., Liu, C.Q., Shields-Zhou, G.A., Jiang, S.Y., 2013. Trace and rare earth element geochemistry of black shale and kerogen in the early Cambrian Niutitang Formation in Guizhou province, South China: constraints for redox environments and origin of metal enrichments. *Precambrian Res.* 225, 218–229.
- Pollack, G.D., Krogstad, E.J., Bekker, A., 2009. U-Th-Pb-REE systematics of organic-rich shales from the ca. 2.15 Ga Sengoma Argillite Formation, Botswana: Evidence for oxidative continental weathering during the Great Oxidation Event. *Chem. Geol.* 260, 172–185.
- Qi, L., Hu, J., Gregoire, D.C., 2000. Determination of trace elements in granites by inductively coupled plasma mass spectrometry. *Talanta* 51, 507–513.
- Qi, F.C., Li, Z.X., Long, Z.Z., Wang, W.Q., Wang, W.G., Yang, Z.Q., Zhang, Y., 2014. The Discovery of onofrite and uraninite in marine phosphorite and its geological significance, Northwestern Hunan. *Uranium Geol.* 30 (3), 129–134.
- Richardson, K.A., 1959. The Thorium, Uranium and Zirconium Concentrations in Bauxites and their Relationship to Bauxite Genesis. The Rice Institute, Houston, Texas 5, 1–55.
- Taylor, S.R., McLennan, S.M., 1985. The Continental Crust: Its Composition and Evolution. Blackwell, Oxford, pp. 1–312.
- Tian, H.Q., Guo, T.L., Hu, D.F., Tang, L.J., Wo, Y.J., Song, L.Y., Yang, Z.Q., 2006. Marine Lower assemblage and exploration prospect of central Guizhou Uplift and its adjacent areas. *J. Palaeogeogr.* 8 (4), 509–518 (In Chinese with English abstract).
- USGS, 2009. Mineral Commodity Summaries: Bauxite and Alumina. United States Government Printing Office, Washington, pp. 1–8.
- Viers, J., Wasserburg, G.J., 2004. Behavior of Sm and Nd in a lateritic soil profile. *Geochim. Cosmochim. Acta* 68, 2043–2054.
- Wang, Q.F., Deng, J., Liu, X.F., Zhang, Q.Z., Sun, S.L., Jiang, C.Z., Zhou, F., 2010. Discovery of the REE minerals and its geological significance in the Quyang bauxite deposit, West Guangxi, China. *J. Asian Earth Sci.* 39, 701–712.
- Wang, Q.F., Liu, X.F., Yan, C.H., Cai, S.H., Li, Z.M., Wang, Y.R., Zhao, J.M., Li, G.J., 2012. Mineralogical and geochemical studies of boron-rich bauxite ore deposits in the Songqi region, SW Henan, China. *Ore Geol. Rev.* 48, 258–270.
- Wang, X.M., Jiao, Y.Q., Du, Y.S., Ling, W.L., Wu, L., Cui, T., Zhou, Q., Jin, Z.G., Lei, Z.Y., Weng, S.F., 2013. REE mobility and Ce anomaly in bauxite deposit of WZD area, Northern Guizhou, China. *J. Geochem. Explor.* 133, 103–117.
- Wang, W.G., 2015. The Discover of Brannerite and Uraninite in Lower Cambrian U-bearing phosphorite in West Hunan. *Uranium Geol.* 31 (1), 19–28.
- Wang, S., Zhang, J., 2016. Mineral and rock composition and resource properties of Lower Cambrian black shale in Zijin, Guizhou Province. *Acta Petrol. ET Mineral.* 3, 543–552.
- Wei, X., Ji, H.B., Li, D.J., Zhang, F.L., Wang, S.J., 2013. Material source analysis and element geochemical research about two types of representative bauxite deposits and terra rossa in western Guangxi, southern China. *J. Geochem. Explor.* 133, 68–87.
- Wu, G., Liu, Y., Zhang, Y., 2006. Geological characters and aluminum ore resources potential in the Wuchuan-Zheng'an-Daozhen area. *Geol. Prospect.* 42, 39–43 (in Chinese with English abstract).
- Yang, R.D., Chen, W., Zhou, R.X., 2012. Characteristics of Organic-rich shale and exploration area of shale gas in Guizhou Provine. *Nat. Gas Geosci.* 23 (2), 340–347 (in Chinese with English abstract).
- Yang, E.L., Lu, X.B., Bao, M., Luo, J.J., Hu, Q.C., 2013. Enrichment and origin of some trace elements in black shales from the early Cambrian in eastern Guizhou Province. *Adv. Earth Sci.* 28 (10), 1160–1169.
- Yang, X.F., Pang, B.C., Chen, Y.B., Zhu, W.F., 2014. Mineral characteristics and metallogenetic mechanism of Heuitian bauxite deposit in central Guizhou. *J. Guilin Univ. Technol.* 34 (1), 15–22 (in Chinese with English abstract).
- Yi, T.S., Zhao, X., 2014. Characteristics and distribution patterns of the Lower Cambrian Niutitang Shale reservoirs in Guizhou. *Chin. 34 (8)*, 1–7 (In Chinese with English abstract).
- Zamanian, H., Ahmadnejad, F., Zaravandi, A., 2016. Mineralogical and geochemical investigations of the Mombi bauxite deposit, Zagros Mountains, Iran. *Chem. Erde Geochem.* 76, 13–37.
- Zarasvandi, A., Charchi, A., Carranza, E.J.M., Alizadeh, B., 2008. Karst bauxite deposits in the Zagros mountain belt, Iran. *Ore Geol. Rev.* 34, 521–532.
- Zhao, K.D., Jiang, S.Y., Chen, P., Chen, R., Ling, H.F., 2014. Mineralogy, geochemistry and ore genesis of the Dawan uranium deposit in southern Hunan Province, South China. *J. Geochem. Explor.* 138, 59–71.
- Zhang, Z.W., Zhou, L.J., Li, Y.J., Wu, C.Q., Zheng, C.F., 2013. The “coal-bauxite-iron”

structure in the ore-bearing rock series as a prospecting indicator for southeastern Guizhou bauxite mines. *Ore Geol. Rev.* 53, 145–158.

Zhang, Y., Yan, D., Zhao, F., Li, X., Qiu, L., Zhang, Y., 2016. Stratigraphic sequences, abundance anomalies and occurrences of As, Sb, Au, Ag in the Lower Cambrian Niutitang Formation in Kaiyang Phosphate Mine area. *Acta Petrol. Sin.* 32 (11),

3252–3268.

Zhou, J., Hu, K., Bian, L.Z., 2008. Geochemical characteristics and ore-forming processes of Ni-Mo polymetallic deposits in Lower Cambrian black shale, Zunyi, Guizhou Province. *Miner. Deposits* 27 (6), 742–750 (In Chinese with English abstract).